Strong Resistance of Citrate Anions on Metal Nanoparticles to Desorption under Thiol Functionalization

Jong-Won Park[†] and Jennifer S. Shumaker-Parry*

Department of Chemistry, University of Utah, 1400 East 315 South, RM 2020, Salt Lake City, Utah 84112, United States. [†]Present address: Department of Chemistry and The Photonics Center, Boston University, Boston, MA 02215.

ABSTRACT Thiols are widely utilized to functionalize metal nanoparticles, including ubiquitous citrate-stabilized gold nanoparticles (AuNPs), for fundamental studies and biomedical applications. For more than two decades, citrate-to-thiol ligand exchange has been used to introduce functionality to AuNPs in the 5−100 nm size regime. Contrary to conventional assumptions about the completion of ligand exchange processes and formation of a uniform self-assembled monolayer (SAM) on the NP surface, coadsorption of thiols with preadsorbed citrates as a mixed layer on AuNPs is demonstrated. Hydrogen bonding between carboxyl moieties primarily is attributed to the strong adsorption of citrate, leading to the formation of a stabilized network that is challenging to displace. In these studies, adsorbed citrates, probed by Fourier transform infrared and X-ray photoelectron spectroscopy (XPS) analyses, remain on the surface following thiol addition to the AuNPs, whereas acetoacetate anions are desorbed. XPS quantitative analysis indicates that the surface density of alkyl and aryl thiolates for AuNPs with an average diameter of ∼40 nm is 50−65% of the value of a close-packed SAM on Au(111). We present a detailed citrate/thiolate coadsorption model that describes this final mixed surface composition. Intermolecular interactions between weakly coordinated oxyanions, such as polyprotic carboxylic acids, can lead to enhanced stability of the metal−ligand interactions, and this needs to be considered in the surface modification of metal nanoparticles by thiols or other anchor groups.

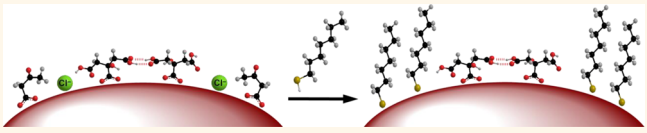

KEYWORDS: gold nanoparticles · citrate displacement · surface coverage · XPS quantitative analysis · ligand exchange · self-assembled monolayer

Due to the critical role of surface organic layers, much effort is put into modifying the surface functional groups to tailor the properties of metal nanoparticles (MNPs). The most commonly used approach for surface modification is thiol functionalization.[1,2] Because thiols have a strong affinity for noble metals and form organized self-assembled monolayers (SAMs) on planar Au surfaces,[3,4] ω-terminated thiols are often used for the formation of robust ligand shells on MNPs.[5,6] Unlike on a pristine planar metal surface, stabilizer ligands are intrinsically present on MNP surfaces after wet-chemical synthesis. To form a well-defined SAM on the surface of MNPs, those stabilizers are inclined to be displaced by incoming thiol ligands through a process called ligand exchange. Citrate-stabilized gold nanoparticles (Cit-AuNPs) are common nanomaterials, and citrate-to-thiol exchanges typically are the first step for a large variety of studies related to the chemical and biological properties of AuNPs in the 5 to 100 nm size range.[7] For the most part, the approach to this ligand exchange is presented in a rather simple manner based on the assumption that the thiol molecules spontaneously displace the citrates, leading to a completely thiolate-functionalized nanoparticle.[5] Statements about ligand exchange of thiolates for citrate molecules on AuNPs[5,6] are made due to the substantial difference in energy between Au−S[8] (∼40 kcal/mol) and Au−O_{COOH}[9] (∼2 kcal/mol) interactions, but other factors impact the ligand exchange process, including kinetic, electronic, steric, chelating, and solvent effects.[10] In a previous study, we found that surface citrate anions (dihydrogen species, H_2Cit^-) form hydrogen-bonded networks on AuNPs[11] as originally speculated by Grieser and co-workers,[12,13] and thus, the resulting steric and chelating effects of the entire citrate layer can govern the citrate-to-thiol exchange, in addition to single bond energies. This suggests that surface

* Address correspondence to shumaker-parry@chem.utah.edu.

Received for review November 7, 2014 and accepted January 21, 2015.

Published online January 27, 2015
10.1021/nn506379m

citrate anions may not be readily displaced by thiols. Until now, however, there have been abundant examples of reports relying on the assumption of complete displacement of the adsorbed citrates by thiols, including Cit-AuNPs conjugated with thiol-linked DNA and TNF (tumor necrosis factor) for clinical use.[14] Remaining citrate molecules impact the NP surface chemistry due to the hydroxyl/carboxyl functionality and influence properties such as pH-dependent surface charge, intracellular activity,[15] and toxicity.[16] Moreover, surface coverage of thiolates on AuNPs can be restricted to a great extent by the citrates already adsorbed on the particle surface.[17] The significant and broad impact motivates the need for a detailed understanding of the displacement of weakly coordinated but hydrogen-bonded polyprotic carboxylic acids, as well as subsequent formation of SAMs through thiol anchor groups on MNPs.

One of the simple tests for citrate-to-thiol exchange has been NP aggregation studies based on UV−visible spectroscopy,[5] where the aggregation characterized by a red shift of a localized surface plasmon resonance (LSPR) is used to follow the adsorption of thiols on AuNPs. This test is associated with the assumption that the displacement of the negatively charged surface ions (*e.g.*, citrate anions) causes AuNP aggregation due to the loss of electrostatic repulsion and colloidal stability in solution.[18] The NP aggregation-based approach has become a representative protocol to monitor replacement of adsorbed citrates on MNPs.[19] This method exclusively relies on an electrostatic mechanism to stabilize the MNPs, rooted in coarsely considering each citrate molecule as a static point charge. However, the direct correlations between citrate desorption, surface charge depletion, and colloidal instability are no longer valid when other ligand layers coadsorbed on NPs drive charge neutralization and/or dominate interparticle interactions. For example, the carboxylate negative charge may be neutralized *via* protonation[20] or cationic molecule adsorption,[12,21] leading to a decline in the surface charge of the particles. Also, interlayer interactions, including hydrogen bonding, electrostatic attraction, and hydrophobic effects, may induce interparticle attraction[22] without the citrates actually being displaced. The colorimetric assay based on NP agglomeration processes is an unpropitious method of studying the replacement of adsorbed citrate by incoming thiols, and molecular spectroscopic methods to probe ligand exchange are warranted to gain an understanding of the process.

Herein, we present experimental evidence that a significant portion of citrate anions remains on AuNPs (~40 nm in diameter) treated with alkyl and aryl thiols in solution based on attenuated total reflectance infrared spectroscopy (ATR-IR) and X-ray photoelectron spectroscopy (XPS) analyses. Owing to the detailed structural characterization of the citrate adlayer in our previous study, we utilize unique spectroscopic signals of H_2Cit^- directly adsorbed on the AuNPs for the surface analysis, which are characterized by the ν(C═O) vibration of carboxylic acid groups through acyclic dimerization at 1734 cm^{-1}, the asymmetric $\nu(COO^-)$ of gold−carboxylate (Au−COO^-) coordination at 1615−1540 cm^{-1}, and the C 1s binding energy of the Au−COO^- species at 288 eV.[11] Surface density of alkyl and aryl thiols on AuNPs was estimated using adsorption isotherm analysis based on Au and S compositions from XPS data. These adsorbate/substrate-based densities are complementary to the ratio of surface coverage of coadsorbed alkanethiolates to pre-existing citrates, determined from a linear regression slope of a plot of the ratio of alkanethiolate C 1s intensities to carboxyl C 1s intensities *versus* the number of the methylene units of alkanethiolates. Both quantitative surface analyses suggest that the surface coverage of aryl and alkyl thiolates on Cit-AuNPs is far less than the commonly assumed value for the formation of SAMs. The composition of a mixed layer of citrate/thiolate ligands on edge and facet surfaces is proposed. The influence of adsorbed alkanedithiolates on adjacent citrates is probed by monitoring the structural transformation of citrate anions, which depends on the hydrocarbon length of dithiolates confined at surface regions free of adsorbed citrate. Contributions from intermolecular interactions between surface citrates are considered in order to explain the strong adsorption of citrate molecules on AuNPs. Finally, a description of the Cit-AuNP surface composition is presented based on analysis of the XPS data considering different Au oxidation states.

RESULTS AND DISCUSSION

IR and XPS Characteristics of Remaining Citrates on AuNPs Functionalized by Alkyl Thiols. ATR-IR and XPS spectroscopic approaches were used to probe coordinated citrate species on AuNPs exposed to methyl-terminated alkanethiol. This type of thiol was chosen because it induces NP aggregation, and the extent of aggregation is often used to study displacement of citrate anions. Also, the presence of the methyl group of the thiol does not interfere in the identification of the carboxylic acid groups of citrate in IR and XPS analyses. Intermolecular interactions between terminal methyl groups of the alkanethiols in ethanol solution are very weak,[23] preventing a multilayer formation of alkanethiol on the AuNP surface. After addition of excess amounts (1 mM ethanolic solution) of 1-dodecanethiol ($CH_3-C_{11}-SH$) into a solution of Cit-AuNPs, AuNPs exhibit a typical broadened LSPR band red-shifted from the plasmon response of the well-dispersed particles due to plasmon coupling in the NP aggregates formed (Figure S1 in the Supporting Information). The concentration of the thiol solution

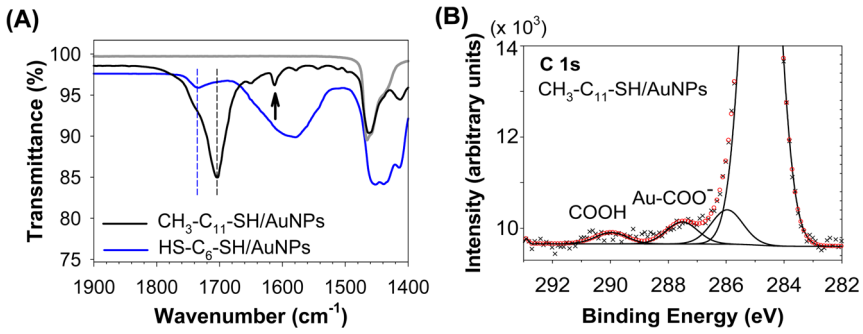

Figure 1. IR and XPS spectra indicative of coordinated citrate species remaining on AuNPs after addition of alkanethiol. (A) ATR-IR spectrum of AuNPs functionalized with dodecanethiol ($CH_3-C_{11}-SH$) exhibits the characteristic ν(C═O) of hydrogen-bonded COOH groups centered at 1704 cm^{-1} (black dashed line) along with $\nu_{asy}(COO^-)$ of surface-coordinated Au−COO at 1611 cm^{-1} (indicated by the arrow). Another ν(C═O) at 1734 cm^{-1} (blue dashed line), which is associated with surface-specific hydrogen bonding, becomes distinct when Cit-AuNPs are functionalized with 1,6-hexanedithiol ($HS-C_6-SH$) (blue spectrum). Also, $\nu_{asy}(COO^-)$ of the central carboxylate of dangling citrates at 1575 cm^{-1} becomes enhanced. The gray spectrum is for pure $CH_3-C_{11}-SH$ without AuNPs, which also represents pure $HS-C_6-SH$ in the given frequency range (corresponding spectrum omitted for clarity). Blue and gray traces are offset from baselines by ±2% for clarity. (B) Deconvoluted XPS C 1s spectrum of AuNPs functionalized with dodecanethiol ($CH_3-C_{11}-SH$) shows coordinated COO^- on Au surfaces at 287.6 eV. Raw data are represented by cross symbols (×), and an envelope spectrum is displayed by red circles (○).

is ∼270 times larger than that needed to saturate the AuNP surfaces. The aggregation of Cit-AuNPs functionalized with thiols has been used ostensibly to assess the complete displacement of citrate anions, but molecular analyses show that citrates remain on the AuNPs even after exposure to high concentrations of thiols.

Remaining surface citrates on AuNPs were identified using IR spectral signatures unique to the adsorbed citrate species, as seen in Figure 1A. IR spectra were recorded for AuNPs after purification using a typical centrifugation procedure and then dried on an ATR substrate (see the Methods). A characteristic ν(C═O) of hydrogen-bonded COOH appearing at 1704 cm^{-1} was monitored for Cit-AuNPs treated with $CH_3-C_{11}-SH$ (black dashed line, black spectrum in Figure 1A). Previously, we assigned this dominant peak to a cyclic COOH dimerization between adsorbed and dangling citrate anions.[11] More importantly, another perceptible ν(C═O) of hydrogen-bonded COOH at 1734 cm^{-1} was also observed (blue dashed line), and this is associated with a surface-specific acyclic dimerization between two adsorbed citrate anions.[11] A deconvoluted spectrum is presented in the Supporting Information (Figure S2). Interactions of alkyl thiolates with dangling citrates possessing configurational flexibility were probed. When Cit-AuNPs were treated with 1,6-hexanedithiol ($HS-C_6-SH$) (blue spectrum in Figure 1A), the transmittance magnitude of the ν(C═O) band at 1704 cm^{-1} was significantly attenuated. In a previous study, we suggested an orientation change of dangling citrate anions with respect to the metal surface.[11] The dithiol ligands with both sulfur atoms bound to the surface may partially disrupt hydrogen-bonded dangling citrates that move outward from the surface through repulsive van der Waals (vdW) forces generated from hydrocarbon backbones in close proximity. As the cyclic COOH dimer orients perpendicular to the surface, the parallel component of the C═O bond dipoles to the metal surface becomes dominant, making the ν(C═O) vibration IR-inactive according to the surface selection rule[24] (Figure S3 in the Supporting Information). However, the transmittance level from the ν(C═O) band at 1734 cm^{-1} does not change drastically, owing to the stabilized orientation of the surface-specific COOH dimerization. The ν(C═O) frequencies of adsorbed citrate species are summarized in the Supporting Information (Table S1). It is unlikely that citrate anions possessing one hydroxyl and three carboxyl groups would become trapped in the hydrophobic layers of the alkanethiolate after being displaced from the AuNP surface. We attribute the presence of these vibrational modes of carboxyl moieties to citrates remaining on the surface of the thiol-functionalized AuNPs.

The existence of remaining surface citrates is further supported by detection of gold−carboxylate coordination.[25] An asymmetric COO^- stretching vibration ($\nu_{asy}(COO^-)$) of a characteristic η^1-COO^- coordinate to Au atoms appears at 1611 cm^{-1} as a small, but sharp, band (indicated by the arrow in Figure 1A). This $\nu_{asy}(\eta^1\text{-}COO^-)$ is ascribed by binding one of the oxygen atoms of a terminal carboxylate to the surface, which discriminates adsorbed citrate from sodium citrate and citric acid that are not associated with a surface. Coordination of two oxygen atoms of the central carboxylate to the surface also produces the frequency of $\nu_{asy}(COO^-)$ at 1540 cm^{-1}. Although the $\nu_{asy}(COO^-)$ vibrational mode is parallel to the AuNP surface and *a priori* IR-forbidden, a dynamic dipole moment *via* carboxylate-to-gold electron transfer[26] can couple with the molecular vibration,[27] and/or the facet surface may not be atomically flat due to the possible existence of Au adatoms,[28] resulting in the appearance of

this mode. Thus, the presence of the Au−COO coordinate is direct evidence of incomplete displacement of citrate by the alkanethiols under typical experimental conditions of ligand exchange reactions. Interestingly, those Au−COO bands become broadened when Cit-AuNPs are functionalized with HS−C_6−SH, probably due to repulsive vdW forces from the lying-down configuration of the likely planar alkanedithiolates[29] impacting the orientation and arrangement of the nearby adsorbed citrates (blue spectrum in Figure 1A; also see deconvoluted spectra in Figure S4 in the Supporting Information). In addition, the other $\nu_{asy}(COO^-)$ peak at 1575 cm^{-1} associated with the central carboxylate group of dangling citrates[11] becomes more intense because the direction of the $\nu_{asy}(COO^-)_{central}$ vibration may be mostly perpendicular to the surface as the dangling citrate anions orient toward the surface normal and, consequently, exhibit strong IR activity (Figure S3 in the Supporting Information).

XPS analysis also provided evidence of remaining surface citrate (Figure 1B). The XPS spectrum of C 1s shows two major peaks at higher binding energies (BEs) of 287−291 eV attributed to carboxyl species compared to the peak for hydrocarbon at 284.8 eV. One C 1s peak at 287.6 eV corresponds to the gold-coordinated carboxylate (Au−$\underline{C}OO^-$),[30] and the other C 1s at 289.4 eV is assigned to the free carboxylic group ($\underline{C}OOH$).[31] The strong peak at 284.8 eV is associated with the aliphatic chain of the thiolate, and the deconvoluted peak at ∼286 eV is attributed to hydroxy-hydrocarbon-based contaminants from air[32] along with contributions from the citrate −$\underline{C}H_2$−/−$\underline{C}$OH and thiolate −$\underline{C}H_2$S− moieties. XPS evidence of the presence of the carboxylate carbon supports the IR analysis and demonstrates that the surface citrate is not completely displaced by the thiol. This finding agrees with the detection of residual citrate anions on Cit-AuNPs treated with thiols (cysteamine) by Cheng and co-workers using laser desorption ionization mass spectrometry (LDI-MS).[33] Lee and co-workers also discussed incomplete displacement of citrate anions on AuNPs after addition of alkanethiols, even for multidentate ligands having more than one thiol moiety.[34] Under conditions without citrate interference by using ligand-free AuNPs, Petersen and Barcikowski demonstrated that conjugation with thiolated oligonucleotides yields a higher surface coverage up to a factor of 5 in comparison to the conventional conjugation to Cit-AuNPs.[17] Therefore, there are multiple indications that ligand exchange reactions of Cit-AuNPs with incoming thiol do not easily lead to complete displacement of citrate, although this is typically assumed to be a facile process.

The remaining citrate in the aggregated AuNPs suggests that the NP aggregation-based assay[5,19] is not adequate to estimate the extent of the replacement of citrate for the studies of ligand exchange

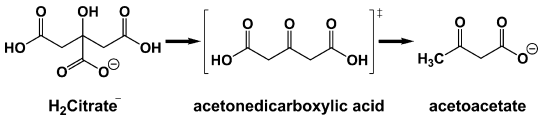

Scheme 1. Oxidation of citrate into acetoacetate *via* two consecutive decarboxylation pathways.

reactions. The aggregation of Cit-AuNPs only implicates thiols in the adsorption on the NP surface, not necessarily the displacement of citrate. In the aforementioned assay, the possibility of the coadsorption of thiols with preadsorbed citrates is neglected. In fact, the interplay of attractive and repulsive interactions between thiolate functional groups and citrate layers can govern the process of NP aggregation (see ref 11 and Figure S5 in the Supporting Information). There have been studies suggesting complete ligand exchange. For example, Epple and co-workers suggested a quantitative displacement of citrate by polyvinylpyrrolidone (PVP) using elemental analyses for carbon, hydrogen, and gold.[35] However, the much smaller molecular weight of citrate compared to the massive size of the PVP used in their study may introduce a challenge in the determination of a precise value for the carbon content of residual citrate because of detection limits for this analysis method. In addition, based on zeta-potential measurements indicating a negative surface charge and the presence of sodium ions, the authors suggested the presence of residual citrate.

In our previous study, we demonstrated that acetoacetate,[36,37] the major oxidized species of citrate during AuNP synthesis,[25] is desorbed from the surface.[11] Two consecutive processes of citrate decarboxylation produce acetoacetate (Scheme 1). Acetonedicarboxylic acid (β-ketoglutaric acid) is not stable in the course of AuNP synthesis.[25,38] While XPS signals for C 1s of citrate Au−COO^- and acetoacetate C═O are overlapped around 288 eV, IR frequencies distinct from citrate can be used for identifying acetoacetate displacement. In that study, we observed that, upon thiol addition to the AuNPs, the intensity of $\nu_{asy}(COO^-)$ at ∼1590 cm^{-1}, mainly emanating from acetoacetate −CH_2COO^- moieties, was drastically attenuated, and a characteristic ν(C═O) of saturated aliphatic ketone at 1725−1710 cm^{-1} disappeared, leaving only the citrate ν(C═O) of hydrogen-bonded COOH groups at 1704 and 1734 cm^{-1} (see both Figure 4 and Figure S11 in ref 11). Acetoacetate can be further oxidized into acetone and acetate[38] (see ref 25 for acetoacetate oxidation pathways), and these final byproducts at the end of citrate oxidation are expected to remain solvated rather than adsorbed on the metal surface due to a lack of a strong driving force for adsorption. Besides acetoacetate, adsorbed citrate species can also exhibit similar IR frequencies at 1711 and 1593 cm^{-1}, ascribed by OH···HOOC/OH···$^-$OOC intramolecular

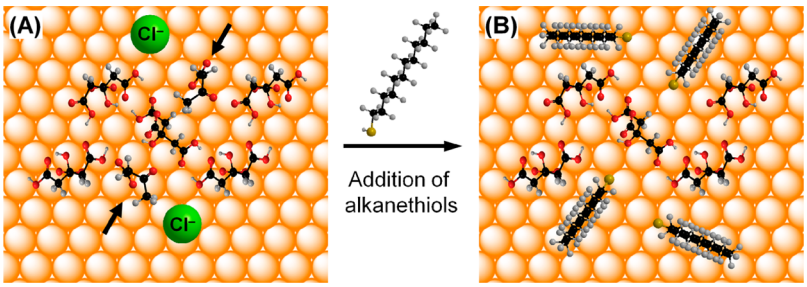

Figure 2. Qualitative perspective of ligand exchange on Cit-AuNPs under thiol functionalization. (A) Representative chemical species of interest on the (111) surface of Cit-AuNPs as prepared. (B) Surface of Cit-AuNPs after thiol ($CH_3-C_{11}-SH$) addition. Adsorption configuration of the alkanethiolates is arbitrary, except the sulfur–sulfur spacing is optimized. Surface gold atoms (orange spheres) and chloride ions (green spheres) are illustrated as a space-filling model, whereas citrate, acetoacetate (indicated by arrows), and alkanethiolate molecules are depicted as a ball-and-stick model. The citrate anion at the center is a dangling species not in direct contact with the surface. Note that the spectroscopy data indicate that hydrogen-bonded citrate molecules remain, but acetoacetate and chloride anions are displaced by the thiols.

interactions, respectively.[11] Although IR features of acetoacetate are largely overlapped with those of adsorbed citrates, except $\nu(C-H)_{CH3}$ frequencies, another ligand exchange performed for AuNPs having only isolated adsorbed citrates indicates that a majority of citrate remains on the surface (see discussion below). Therefore, we concluded that the primary organic anion desorbed from the surface is acetoacetate.

Under alkaline conditions, citrate anions are adsorbed on the AuNP surface through a deprotonated form of Cit^{3-}.[11] The central carboxylate group primarily binds to the surface, and only one of the two terminal carboxylate groups can additionally bind to the surface through η^1-coordination, resulting in mono- or bidentate citrate. Upon purification of as-prepared AuNPs with an OH^- solution at pH ~9, a substantial decrease of the $\nu(C-H)$ intensities for acetoacetate $CH_3CH_2^-$ fragments was observed, implicating citrate anions as the primary organic species remaining on the AuNPs. Also, the apparent Au(I)/Au(0) ratio of XPS Au 4f intensities increased from 0.06 to 0.09, and this suggests that a large fraction of surface gold atoms was oxidized to the Au(I) state due to the formation of Au–O *via* binding of OH^-[39,40] or citrate COO^- to the gold surface. The adsorption strength of citrate anions may be enhanced through the ancillary Au(I)–COO^- (terminal) complexation. When a solution of alkanethiol is added to the deprotonated Cit-AuNPs, the peak indicative of the surface-specific COOH dimerization *via* protonation of the terminal carboxyl groups appears at 1734 cm^{-1} with 80% amplitude compared to the peak intensity prior to the deprotonation process.[11] This indicates that even deprotonated species of citrate anions readily form hydrogen bonds under thiol functionalization, presumably through proton transfer from sulfur hydrogen to citrate carboxylate. If surface hydrogen bonding through M–OH···$^-$OOC interactions occurred, the AuNPs would exhibit both $\nu(O-H)_{AuOH}$ at ~3550 cm^{-1}[41] and $\nu(C{=}O)$ at ~1740 cm^{-1}.[42] The former band was not observed in this condition, and thus, the possibility of M–OH···$^-$OOC hydrogen bonding was ruled out. The citrate anions form a robust surface layer, resulting in incoming thiols displacing only a small fraction of citrate anions, likely to a greater extent at edge and vertex sites of the AuNPs.

In addition to the molecular anion, XPS Cl spectra indicate that another negatively charged species displaced from AuNPs is the chloride ion. Peaks in the XPS Cl spectra appear at ~270 eV for Cl 2s[43] and at ~200 eV for Cl 2p.[44,45] Upon addition of the ethanolic solution of $CH_3-C_{11}-SH$ to Cit-AuNPs, those Cl peaks disappear, indicating the displacement of surface chloride ions (Figure S6 in the Supporting Information). There are two major Cl $2p_{3/2}$ peaks at 197.9 and 200.3 eV (Figure S7 in the Supporting Information). The former is associated with Na^+Cl^- and/or Au(I)–Cl^- species, and the latter, which is higher than those of Cl atoms and chloride ions typically at 197–199 eV,[44,45] may be attributed to Au(0)–Cl^- species. We will discuss the presence of chloride ions adsorbed on metallic gold surfaces at the end of this study. It is not clear whether chloride ions are desorbed from the surface in the form of chloride ions or gold–chloride complexes. The footprint of a single citrate anion in the hydrogen-bonded layer is 59 $Å^2$.[11] Since a citrate anion of fully extended conformation fits at a vacant area in the citrate network, resulting in an approximate dimension of 45 $Å^2$ for an extended citrate anion, the fractional surface coverage relative to the Au atom lattice defining a unit cell area of 179 $Å^2$ is 0.75 ML (θ_{Cit} = 1/6 for 1 ML defined by η^2-COO^- coordination on a (111) surface; *i.e.*, two oxygen atoms per COO^- occupied on every six gold atoms, in reference to one sulfur atom of a thiol molecule, are occupied on three gold atoms, yielding θ_{Thiol} = 1/3 for 1 ML) for hydrogen-bonded citrate species. Other surface sites are likely occupied by acetoacetate, non-hydrogen-bonded citrate, and chloride ions. Figure 2 presents a qualitative representation of the displacement of surface anions (acetoacetate and chloride ions) on Cit-AuNPs upon thiol addition.

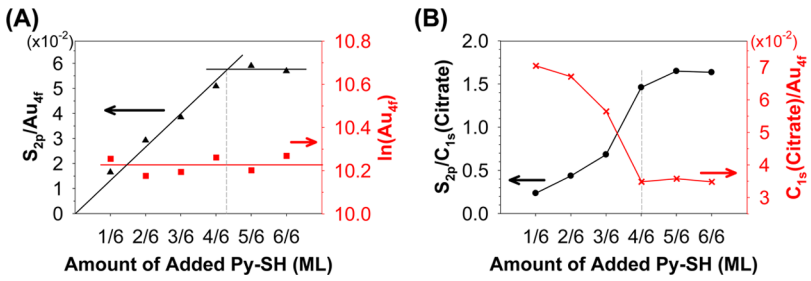

Figure 3. Relationship between the amount of Py−SH in solution and the amount of Py−SH adsorbed on Cit-AuNP surfaces determined from XPS analysis. (A) Apparent ratios of the peak areas of S 2p and Au 4f (▲) as well as peak intensities of Au 4f on a logarithmic scale (■) for different Py−SH solution concentrations. The dotted line guides coverage saturation at 0.7 ML as an upper limit. (B) Ratios of the peak areas of S 2p and citrate C 1s at 288 eV (●) as well as citrate C_{1s}/Au_{4f} (×). Acetoacetate contributes to the intensity of the citrate C 1s, particularly prior to 2/3 ML. The dotted line is a guide at the solution concentration of 2/3 ML.

Adsorption Isotherm of Aryl Thiols for Determination of Surface Area Available for Adsorption in the Presence of Surface Citrates. The adsorption of arylthiols on Cit-AuNPs was studied by XPS analysis. The XPS spectral signatures provide the basis for a semiquantitative assessment of thiolate adsorption and citrate displacement processes. Densely packed AuNPs on a silicon substrate were used for the XPS measurements. Because of a limited penetration depth originating from the inelastic mean free path (IMFP) of gold (λ = 1.55 nm),[46] the XPS signals were collected from the rough surfaces of topmost AuNPs (3λ = 4.65 nm). To plot adsorption isotherms for 4-mercaptopyridine (Py−SH) on Cit-AuNPs, the elemental ratios and atomic compositions were obtained from XPS peak areas at characteristic binding energies, which are the C 1s of the gold−citrate coordinate (Au−COO^-) at 288 eV, the S 2p of pyridine thiolate, and the Au 4f. Typical BE values of S $2p_{3/2}$ and Au $4f_{7/2}$ are 162 and 84 eV, respectively.[2] The average diameter of Cit-AuNPs obtained by TEM analysis is 39 nm (±25%), but the surface area and concentration of AuNPs were calculated using a diameter of 35 nm and corresponding to an extinction coefficient of 6.1×10^9 M^{-1} cm^{-1}, so that a resulting value of adsorption saturation would be closer to an upper limit for the particle population (see the Methods). Monolayer (ML) coverage was defined based on a packing density of 4.3×10^{14} thiolates/cm^2, which was estimated by STM images of benzenethiolate adsorbed on a planar Au(111) surface.[47]

In Figure 3A, ratios relating the surface composition of the adsorbed thiolate to the amount of thiol added to the AuNP solution are plotted. Thiol solution concentrations were varied from 1/6 to 1 ML coverage on the entire AuNP surface, up to 8.6 μM. The thiol adsorption exhibits saturation behavior prior to 1 ML solution concentration. The ratio of S_{2p}/Au_{4f} increases as the amount of added Py−SH increases up to 5/6 ML, showing a linear relationship between the amount of adsorbed thiolate and the thiol concentration in solution. The adsorption saturation can be set at 4.2/6 ML (*i.e.*, 0.70 ML) where pre- and post-saturation lines intersect. As expected, the peak areas of Au 4f are constant over the thiol concentrations, and the S_{2p}/N_{1s} ratios are independent of thiol coverage (Figure S8 in the Supporting Information). This consistency in the adsorption isotherm supports the XPS-based quantitation of adsorbed thiolate in this study.

Figure 3B presents a plot for S_{2p}/C_{1s} displaying a similar adsorption isotherm to that of S_{2p}/Au_{4f}, except the observed composition ratio follows a sigmoidal curve. The sigmoidal profile implicates an influence of citrate or its oxidized species in the adsorption of Py−SH, and this can be rationalized with desorption of acetoacetate. The C 1s BE of the carbonyl carbon of ketone is overlapped with that for Au−COO^- at ~288 eV.[48] These C 1s intensities decrease as S 2p intensities increase up to ~2/3 ML solution concentration, where adsorption saturation of the thiol is achieved. Beyond the saturation point, however, the C 1s intensities remain unchanged. This is consistent with thiol coadsorption displacing acetoacetate and possibly non-hydrogen-bonded citrate anions, leaving vacant areas where citrate anions did not form a network layer. If thiol molecules completely displace citrate anions from the AuNP surfaces, the S_{2p}/C_{1s} ratio would increase exponentially beyond 1/2 ML due to the substantial sulfur content of the aryl thiolate. The correspondence of the saturation points determined by the atomic compositions of S 2p and citrate C 1s demonstrates thiolate/citrate coadsorption. The value of C_{1s}(citrate)/Au_{4f} at the initial stage of the Py−SH functionalization is twice that of the observed minimum value, and this is approximately equivalent to two desorbed species of acetoacetate or non-hydrogen-bonded citrate anions per three hydrogen-bonded citrate anions. This extent of ligand exchange is in good agreement with the surface composition of citrate-related species, for which XPS analysis of C 1s spectra for as-prepared Cit-AuNPs resulted in a ratio of deprotonated acetoacetate to H_2Cit^- anions of ~1.2.[11] In addition, chloride ions are not detected even at 1/6 ML thiol, indicating that ethanol can displace them (Figure S9 in the Supporting Information). C 1s, S 2p,

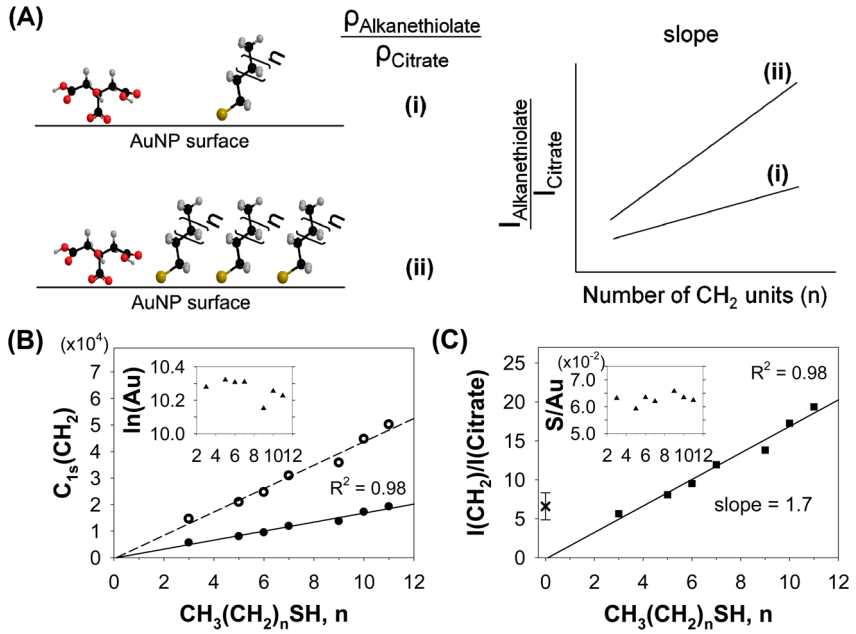

Figure 4. XPS quantitative analyses of the surface coverage ratio of alkanethiol to citrate on AuNPs. (A) Schematic illustration of the relationship between the surface density ratio of alkanethiolate to citrate and the slope of the intensity ratio plot *versus* the number of methylene units. At a given surface density of citrate, the slope value for a lower surface density of thiolate (i) is smaller compared to a higher surface density of thiolate (ii). (B) Intensity of the C 1s peak of methylene moieties at 284.8 eV with respect to the length of alkanethiolates, which exhibits a linear dependence on the hydrocarbon length. A set of open circles (○) with the fitted dashed line represents raw data, and a set of closed circles (●) with the solid line represents normalized intensities of C 1s after the contribution from hydrocarbon impurities is subtracted. Inset: Intensity of Au 4f on a logarithmic scale. (C) Plot of the intensity ratio of the C 1s peak for alkanethiolates/citrates with respect to the length of the alkanethiolate. The slope (1.7) directly represents the ratio of the surface density. Inset: Apparent S_{2p}/Au_{4f} intensity ratio with respect to hydrocarbon length. The ratio at $n = 0$ with an error bar represents purified Cit-AuNPs for comparison (×).

N 1s, and Au 4f spectra used in the XPS analyses are presented in the Supporting Information (Figure S10).

Both adsorption isotherms in Figure 3 illustrate a saturation of Py−SH adsorption on Cit-AuNPs at 0.7 ML as an upper limit, and thus, the packing density of Py−SH is less than 3.0 thiolates/nm^2. The established saturation accounts for both kinetic effects of the ligand exchange process as well as established equilibria, that is, a Langmuir-type model representing the adsorption/desorption equilibrium.[49] Even at these diluted solution concentrations, the surface coverage is comparable with that observed for 1 mM concentration, which will be discussed later. If the diameter of the AuNP sphere considered is increased from 35 nm to the average measured value of 39 nm, this results in a packing density of 2.4 thiolates/nm^2, which is almost one-half of that measured for a planar Au(111) surface (4.3×10^{14} thiolates/cm^2). Adsorption saturation prior to 1 ML suggests that close-packed SAM formation of only thiols cannot be achieved on Cit-AuNPs, in contrast to what is conventionally assumed from thiol functionalization on pristine planar surfaces. Zachariah and co-workers measured the layer thickness of 11-mercaptoundecanoic acid adsorbed on 30 nm Cit-AuNPs, which is 35% less than the predicted value, and they speculated that the thiolate layer on AuNPs is less dense than closely packed SAMs.[50] Based on our results, this observation can be explained by lower surface coverage of the adsorbed thiolate than expected due to partial occupation of AuNP surfaces by citrate that is not readily displaced.

Quantitative Determination of Surface Coverage of Citrates and Thiolates by XPS Analysis. The fractional surface coverage of citrates and alkanethiolates was estimated using a quantitative approach to analyze XPS data. This approach is based on plotting intensity ratios of alkanethiolates to remaining citrates with respect to varied alkanethiol length upon addition of excess thiols[11] (Figure 4A). Thus, the surface functionalization of the AuNPs should be at a saturation level for all chain lengths. The adsorbate/adsorbate ratio-based determination of surface coverage allows for estimating a narrow range of packing density values. This analysis is complementary to the adsorbate/substrate (*i.e.*, sulfur/gold) ratio-based measurements which are limited by the challenge of accurately estimating the calculated surface area as well as the reliance upon defining monolayer coverage by planar reference surfaces that do not adequately represent the nanoparticle surface.

Intensities of 1-alkanethiolates and citrates were determined from integrating the peak areas of C 1s at 284.8 eV for methylene moieties of alkanethiolates and C 1s at 288 eV for coordinated carboxylate groups of citrates. Although the latter typically exhibits a weak signal, the band's intensity is appreciable throughout AuNP samples owing to the high sensitivity of XPS to

subtle amounts of surface species. Notably, the intensity ratios of C 1s of carboxyl carbons at 287−291 eV to Au 4f are similar for Cit-AuNPs before and after thiol functionalization (Table S2 in the Supporting Information). When the surface density of citrate anions is considered ($\theta_{Cit} \sim 75\%$ compared to the estimated monolayer coverage of citrate anions), however, the C 1s intensity of citrate carboxyl carbons is relatively low. For comparison, we functionalized Cit-AuNPs with carboxylic-acid-terminated alkanethiols (COOH−C_n−SH, $n = 2$ and 10) and examined the intensities of the C 1s of carboxyl carbons at 287−291 eV. While the S_{2p}/Au_{4f} ratios are similar to those of the AuNPs functionalized with methyl-terminated alkanethiols, C_{1s}(carboxyl)/Au_{4f} values are significantly larger (250−450% increase) for the carboxylic-acid-terminated alkanethiols (see Table S2). This suggests that the XPS intensity of carboxyl carbon may be orientation-dependent,[51] considering that the plane of citrate carboxyl atoms is approximately parallel to the surface, whereas that of thiolate carboxyl atoms is likely perpendicular to the surface. The latter seems to produce intense C 1s signals of carboxyl carbons. For Cit-AuNPs functionalized with methyl-terminated alkanethiols, however, the C 1s intensities of Au−COO^- coordinated at 288 eV did not fluctuate and, therefore, were used to assess changes in the relative carbon amounts of citrate. C 1s, S 2p, and Au 4f XPS spectra used in the determination of peak intensities are presented in the Supporting Information (Figure S11).

The intensity (I) of the XPS peak is proportional to the surface density (ρ):

$$I_{alkanethiolate} = a \cdot \sigma_{CH2} \cdot \rho_{alkanethiolate} \quad (1)$$

$$I_{citrate} = a \cdot \sigma_{COO^-} \cdot \rho_{citrate} \quad (2)$$

where the term a accounts for factors relating to the source, the spectrometer, and some sample-specific parameters, and the latter two terms $\sigma \cdot \rho$ are chemical-specific factors of interest in this quantitation.[52] The term σ is the photoelectron cross section of carbon atoms, and we assume that $\sigma(CH_2) = \sigma(COO^-)$ for this analysis. The factor (a) also comprises possible intensity deviations due to NP shape effects, although the impact of shape should be minimized by averaging the signal over the rough surface area, which is large compared to that of the individual NPs. Castner and coworkers investigated the layer thickness of SAMs on large AuNPs by XPS analyses,[53,54] and deviations of measured XPS intensities at a certain photoelectron emission angle were negligible among these samples of randomly dispersed NPs.[46,53] The reproducibility of these XPS data is consistent with the high precision of our XPS measurements for Py−SH adsorption on the rough AuNP surface (Figure 3).

The plot of alkanethiolate intensities as a function of the number of methylene units of the alkanethiolates (n) is expected to show a linear relationship for short chain lengths ($n \leq 11$). Accordingly, the following simple relationship can be derived:

$$I_{alkanethiolate,\, n} = (a \cdot \sigma_{CH2} \cdot \rho_{alkanethiolate})n + c_1 \quad (3)$$

where c_1 is a positive constant originating from the XPS intensity due to the methyl groups. In an ambient condition of sample preparation, adsorbed hydrocarbon impurities[52] also contribute to the C 1s signal at 284.8 eV. Thus, the measured intensity of C 1s at 284.8 eV is

$$I_{CH2,\, n} = I_{alkanethiolate,\, n} + I_{impurity} \quad (4)$$

Figure 4B presents a plot of $I_{CH2,n}$ *versus* the number of methylene units. While the intensity of methylene moieties linearly increases as the chain length n increases (open circles and dashed line), the intensity of Au 4f remains constant (inset, Figure 4B). The value of ln(Au_{4f}) is the same as that for Cit-AuNPs functionalized with Py−SH (Figure 3A). Typically, the ln(Au_{4f}) intensity linearly decreases as a function of hydrocarbon length for the closely packed monolayer of alkanethiolates on planar gold surfaces, due to the effect of photoelectron attenuation of Au 4f within the overlayers.[55] The lack of significant attenuation of Au 4f photoelectrons is additional evidence of the formation of a less dense layer of alkanethiolates on the AuNPs, which is the consequence of the presence of preadsorbed citrates. Also, a plot of the ratio of C to Au also produces a linear relationship due to the negligible attenuation of Au intensities (Figure S12 in the Supporting Information).

To extract the alkanethiolate contribution to the apparent C 1s signals, we normalized the C 1s intensities with the atomic composition of sulfur. When the relative C 1s intensities are divided by S 2p intensities, the resulting slope in the plot of C_{1s}/S_{2p} against a methylene unit should be unity. However, a slope of 2.6 was obtained (Figure S13 in the Supporting Information), and thus, an additional 160% of the C 1s signal in this study is coming from sources other than alkanethiolates. The main source is likely hydrocarbon contamination.[52] A possibility of unbound alkanethiols interdigitated in the chemisorbed thiolate layer was excluded due to a lack of S $2p_{3/2}$ at 163−164 eV for free thiol molecules,[2] which is in agreement with the weak intermolecular interactions between methyl-terminated thiols in ethanolic solutions, making this type of layer formation unlikely.[23] Other sources may affect the additional C 1s signals and the negative intercept, including the effects of the roughness associated with the uppermost surface of AuNP aggregates[56] and a length-dependent orientation change of the thiolate layer[57] (see the Supporting Information). The measured intensities of C 1s were divided by the empirical factor of 2.6, and the normalized intensities of alkanethiolates are presented in Figure 4B (closed circles and solid line).

With this correction, the 1:1 relationship between the hydrocarbon density of alkanethiolates and the C 1s signal is still valid for eq 3. Dividing eq 3 by $I_{citrate}$, the relationship between the intensity ratio and the density ratio is given by

$$\frac{I_{CH2,\,n}}{I_{citrate}} = \frac{\rho_{alkanethiolate}}{\rho_{citrate}} n + c_2 (c_2 > 0) \qquad (5)$$

Figure 4C presents the relationship between the ratios in eq 5, and a plot yields a linear fit with a slope (r) of 1.7. The slope directly represents the ratio of the surface density of thiolates to citrates adsorbed on the AuNP surfaces, as illustrated in Figure 4A, and therefore, the ratio is citrate/thiolate = 1:1.7. This is another indication that a substantial amount of citrate remains on the surface after the ligand exchange reaction. Note that the measured S/Au ratio is a constant value regardless of the chain length[53] (inset, Figure 4B), indicating that there is no chain length dependence of surface coverage of alkanethiolates at least up to dodecanethiol in this study. While the intensity of the citrate C 1s signal increases as the length of coadsorbed alkanethiolates increases (Figure S14 in the Supporting Information), the lowest value of citrate C 1s for the shortest alkanethiolate (n = 3) was incorporated into eq 5 as a constant value of the citrate intensity. The reason for this is that the increase in the citrate C 1s amplitude likely originates from the structural change of adsorbed citrate anions rather than an increase of surface density because the surface atomic composition of sulfur does not change. As the hydrogen-bonded COOH groups are transformed into η^1-COO^- binding to the surface, consistent with the enhanced intensity of $\nu_{asy}(\eta^1\text{-}COO^-)$ (Figure S15 in the Supporting Information), the C 1s intensities of Au−COO^- coordination at 288 eV proportionally increase as the alkylthiol chain length increases. For Cit-AuNPs purified by alkaline water, the C 1s intensity ratio is relatively large due to the binding of terminal carboxylate groups to the surface (n = 0 in Figure 4C).[11] Therefore, the determined value of the slope is close to an upper limit, which reflects the configuration of citrate layers having the largest degree of COOH hydrogen bonding between citrate anions in the presence of thiolate layers (Figure S16 in the Supporting Information). The increased population of the η^1-COO^- binding in the presence of the hydrocarbon chain suggests that the adsorption of the alkanethiolate has an impact on the configuration of the citrate, which is evidence for the formation of a somewhat mixed citrate/thiolate layer rather than larger, more distinct domains of each ligand type. Using the alkanethiolate footprint on Au(111) of 22 Å^2 and assuming the footprint of an extended H_2Cit^- anion of 45 Å^2, the packing density of alkanethiolate on the AuNPs is only 0.45 ML (*i.e.*, 2.0 alkanethiolates/nm^2). Although the obtained value of surface coverage of alkanethiolate is precise, the value's accuracy is dependent on the citrate footprint assumed. Therefore, we compare this coverage value with that determined from another XPS analysis based on a gold/sulfur atomic ratio.

A simple formula was derived to determine surface composition of sulfur atoms on AuNPs, through normalizing Au 4f intensity for an apparent value of S_{2p}/Au_{4f} ratio. Owing to the IMFP of 1.55 nm for gold under Al Kα excitation, the Au 4f signal includes a large contribution from the metallic core beneath the outermost surface (typical sampling depth, 3λ = 4.65 nm). If the fractional contribution from surface Au atoms (Au_{surf}) to the total Au 4f intensity is quantified, the resulting ratio of S/Au_{surf} can be used to assess surface coverage (θ) based on the atomic composition ratio S/Au_{surf} = 1/3 for a monolayer coverage.[58] Thus, an equation for the composition ratio of sulfur atoms (S_{NP}) to topmost gold layers ($Au_{surf,NP}$) can be derived for AuNPs:

$$\frac{S_{NP}}{Au_{surf,\,NP}} = \frac{1}{f_{Au}} \frac{S}{Au} \qquad (6)$$

where the term f_{Au} is an XPS signal fraction of topmost gold atoms,[59] and S/Au is an apparent composition ratio derived from peak areas with correction for sensitivity factors. For example, measured values of S/Au ratios for thiolate monolayers on planar gold surfaces in the literature[53] imply that only 13% of Au 4f signals should come from the topmost gold layer, leading to $f_{Au,planar}$ = 0.13, which results in (1/0.13) × S/Au = 0.33 for a monolayer coverage. For AuNPs, we concluded $f_{Au,NP}$ = 0.33 by analyzing reported values of S/Au for the thiolate monolayer on *citrate-free* AuNPs of similar sizes in the literature, wherein citrate anions were not introduced in the course of NP synthesis and surface functionalization.[60,61] A detailed comparison of S/Au values with XPS instruments and experimental parameters is presented in the Supporting Information (Table S3). The f_{Au} = 0.33 is an empirically determined value, but it can be evaluated theoretically by a geometric ratio of surface area between a hemisphere of NPs and a planar surface,[56] $f_{Au,NP} = f_{Au,planar} \times (2\pi R^2/\pi R^2)$ = 0.26 (Figure S17 in the Supporting Information). This fraction deficiency compared to the empirical value may result from X-ray shadowing effects for surface sulfur atoms.[56] Based on eq 6 with $f_{Au,NP}$ = 0.33, the apparent value of S/Au = 0.0628 for AuNPs functionalized with methyl-terminated alkanethiols in this study was converted to θ = 0.19 (0.57 ML), which is in accordance with the previously determined value of 0.45 ML based on the citrate/alkanethiolate coverage ratio. Under Al Kα excitation and common emission angle of photoelectron detection, eq 6 with $f_{Au,NP}$ = 0.33 can be applied without adjustment for large AuNPs with a diameter range of ≥20 nm due to the similar surface to volume ratio.[46,59]

By incorporating the apparent S/Au value for Py−SH adsorbed on Cit-AuNPs into eq 6 and $f_{Au,NP}$ = 0.33,

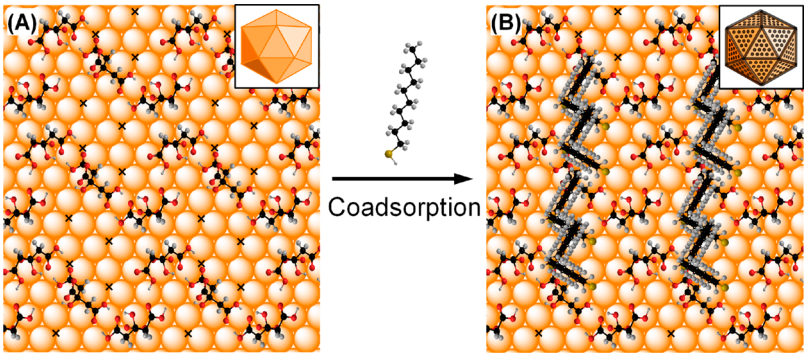

Figure 5. Structural model of coadsorbed citrate and alkanethiolate layers on a AuNP (111) surface in nanometer-scale domains. (A) Representative AuNP surface displaying only hydrogen-bonded citrate layers. Vacant areas are occupied by acetoacetate, chloride, and non-hydrogen-bonded citrate, which are omitted for clarity. Surface gold atoms (orange spheres) on a (111) surface are illustrated as a space-filling model, whereas citrate and alkanethiolate molecules are depicted as a ball-and-stick model. Cross (×) symbols represent the common ($\sqrt{3} \times \sqrt{3}$)*R*30° alkanethiol lattice at accessible three-fold hollow sites. (B) Proposed alkanethiolate (CH_3-C_9-S-) layers on the AuNP surface retaining citrate anions. Note that there is a maximum of four alkanethiolates adsorbed in a vacant site, surrounded by the ideal network of citrate anions. An additional single thiolate molecule can adsorb in the unit cell, depending on the extent of interference by dangling citrate species. A similar coadsorption model is expected on a AuNP (100) surface. Inset: An entire surface of icosahedral Cit-AuNPs functionalized by alkanethiol. Black areas on the surface represent adsorption sites of sulfur atoms of thiol ligands. Each black dot in the facets consists of approximately four thiolate molecules, and other facet areas are occupied by citrates. Edge/vertex areas are covered by close-packed thiolate layers. Scaled approximately for a AuNP with a diameter of 15 nm.

the packing density of 1.9 thiolates/nm^2 is obtained. This is in good agreement with the packing density of Py−S$^-$ thiolate (2.4 thiolates/nm^2, 0.53 ML) estimated previously by adsorption isotherm analysis in this study. Thiolate packing densities of AuNPs functionalized with other types of thiols are summarized in the Supporting Information (Table S4). The coverage values range from 0.52 to 0.64 ML, most likely depending on the interaction between thiol functional groups and citrate layers rather than hydrocarbon chain length or thiol type. It is worth mentioning that thiolate surface coverage does not increase for AuNPs dispersed in solution without aggregation (see Figure S5 and Table S4). Carboxyl-functionalized AuNPs show the highest value of surface coverage (0.64 ML), although those AuNPs aggregated spontaneously upon addition of thiols. Certain types of thiols, which did not induce NP aggregation in 1 mM ethanol solutions for more than 2 h, such as $CH_3O-(EG)_4-C_{11}-SH$ and $NO_2-Ph-SH$, do not produce higher surface coverages (0.64 and 0.59 ML, respectively). Therefore, NP aggregation and possible blockage of adsorption sites on the surface of the NPs cannot be the reason for the incomplete citrate displacement.

The surface coverage of alkyl and aryl thiolates on AuNPs obtained in this study is in accordance with the reported values in literature. The alkanethiolate density on 42 nm Cit-AuNPs determined from the ninhydrin-based assay by Xia and co-workers is 2.2 thiolates/nm^2.[62] The density of 3.4 arylthiolates/nm^2 for 13 nm Cit-AuNPs was obtained by Zhang and co-workers, determined from adsorption isotherm analysis.[63] This slightly large value may be attributed to the smaller size of AuNPs having more contributions from edge and vertex surfaces as well as probably due to a slight deviation in AuNP surface area determination, similar to our initial result of Py−SH packing density (3.0 thiolates/nm^2) based on adsorption isotherm experiments. Typically, the packing density of ~6 thiolates/nm^2 is observed for small gold crystals with a diameter of 3 nm,[64,65] where the effect of nanoparticle curvature due to edge and vertex sites significantly elevates the thiolate coverage from the common value of 4.5 thiolates/nm^2 on planar gold surfaces.[2] The upper limit of packing density of a close-packed SAM of alkanethiolates on the entire surface of a 10 nm icosahedron AuNP is 5.3 thiolates/nm^2, whereas the value is 4.8 thiolates/nm^2 for a 40 nm AuNP.[65] Considering the significant amount of remaining citrate anions, a packing density of thiolates on Cit-AuNPs should be much lower than the value for a close-packed SAM on AuNPs. Our results are in accordance with other experimental reports suggesting a less dense layer of alkanethiolates on Cit-AuNPs.[50,66]

Model of Thiolate Coadsorption with a Hydrogen-Bonded Citrate Network on the AuNP Surface. Figure 5 presents a model of alkanethiolate adsorption on Au(111) used to explain the measured thiolate/citrate ratio of 1.7. At the vacant surface in a fully hydrogen-bonded citrate network,[11] there are approximately four theefold hollow sites contingent on the common ($\sqrt{3} \times \sqrt{3}$)*R*30° alkanethiol lattice. In other words, in the unit cell possessing two Au−COO fragments, four thiolate molecules can bind to the surface. This structure-based model provides a maximum ratio of alkanethiolate to adsorbed citrate species of 2.0 on Au(111). The estimated structures of citrate layers on (110) and (100) surfaces, which are the most common facets together with the (111) surface for large AuNPs, are similar to that on the (111) surface.[11] Although surface coverage

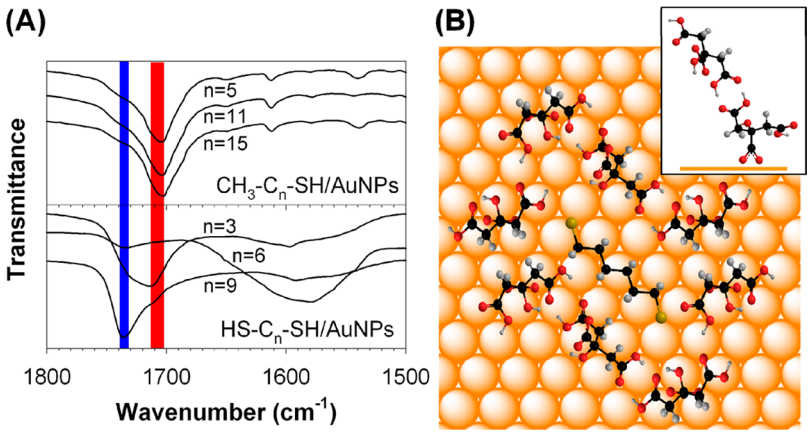

Figure 6. Repulsive van der Waals forces between adsorbed alkanedithiolates and the citrate layer network on a AuNP surface. (A) IR spectra in the regions of ν(C═O) and ν_{asy}(COO^-) for citrate layers on AuNPs after addition of alkanethiols (CH_3-C_n-SH, n = 5, 11, 15) and alkanedithiols ($HS-C_n-SH$, n = 3, 6, 9). Red and blue shaded regions highlight the ν(C═O) of the cyclic COOH dimerization associated with dangling citrate at 1704 cm^{-1} and the ν(C═O) of the surface-specific acyclic COOH dimerization at 1734 cm^{-1}, respectively. Spectra for alkanethiolates/AuNPs exhibit an identical feature regardless of chain length, whereas those for alkanedithiolates exhibit a nonmonotonic feature depending on chain length. The spectral features reflect the degree to which thiolate hydrocarbons exert vdW repulsion over the citrate layer, indicated by a subsequent orientation of dangling citrate. Spectrum traces are offset for comparison. (B) Structure-based model of coadsorbed $HS-C_6-SH$ confined on a vacant site in the hydrogen-bonded citrate network on a AuNP (111) surface. Adsorption of alkanedithiolate and subsequent vdW interactions leads to partial disruption of citrate hydrogen bonds and results in a standing-up configuration of dangling citrate (inset). This force is maximized for $HS-C_6-SH$ transiently confined, which is consistent with its unique IR spectrum. The vdW force from alkanethiolates is mainly governed by collective adsorption *via* single Au−S bonds in the vacant area, and this is not distinct among different chain lengths. Surface gold atoms (orange spheres) on a (111) surface are illustrated as a space-filling model, whereas citrate and alkanedithiolate molecules are depicted as a ball-and-stick model.

of alkanethiols on Au(100) (6.0 thiolates/nm^2)[67] is much larger than the value on Au(111) (4.5 thiolates/nm^2), vacant areas between hydrogen-bonded citrate networks limit the extent of surface area available for adsorption of thiol molecules. Those vacant areas are expected to be similar on Au(111) and Au(100), and the maximum coverage ratio on the (100) surface of the AuNPs is potentially closer to 2.0. Therefore, the thiolates are loosely packed on the facet surfaces, where four thiolate molecules may be coadsorbed with one dangling and two adsorbed citrate anions in the unit cell area of 1.79 nm^2,[11] resulting in a packing density of 2.2 alkanethiolate/nm^2. The theoretical values for facets are smaller than the experimentally determined value of 2.6 alkanethiolate/nm^2 for the entire surface of AuNPs, and therefore, thiolates may form a denser layer in edge or vertex areas. The coverage discrepancy has been resolved by incorporating ~10% surface area, which is likely an approximate fraction of edge and vertex areas,[68] with 6.0 thiolates/nm^2 into calculating thiolate packing density for the entire AuNP surface. Without dangling citrates, one thiol molecule may be adsorbed additively on facets. A predicted upper limit of packing density of thiolates on 40 nm Cit-AuNPs is 3.1 thiolates/nm^2 (0.69 ML), estimated using the larger packing density on edge/vertex surfaces and assuming adsorption of five thiol molecules in the unit cell of facet surfaces without interference from dangling citrate anions (see Table S4 for thiol coverage range). In conclusion, the structure-based model of citrate layers provides a basis for predictable packing density and molecular-level description of thiol adsorption on AuNPs.

Additional evidence for adsorption of thiolates in surface regions lacking a stabilized citrate network comes from analysis of the adsorption of dithiols on the AuNP surface. Interestingly, IR data provide evidence that dithiolate adsorption leads to an orientation change of dangling citrate anions, and this is alkanedithiol-length-dependent. The molecular length dependence of dithiol adsorption can be correlated with the size of the vacant area in the citrate network. While adsorption of methyl-terminated alkanethiolate exhibits a similar feature of ν(C═O) and ν(COO^-) bands regardless of chain length, alkanedithiol adsorption significantly alters the shape and intensity of those bands depending on chain length (Figure 6A). We interpreted this nonmonotonic IR feature using the model of citrate layers. For alkanethiolate adsorption, the Au−COO bond and the overall configuration of the citrate network do not change due to the weak interaction between citrates and hydrocarbon chains. The collective vdW force from alkanethiolates may not be distinct among different chain lengths due to a similar standing-up configuration *via* single Au−S bonds in the vacant area. In contrast with alkanethiolate having one sulfur atom, both sulfur atoms of dithiols can be adsorbed on the surface, resulting in a lying-down configuration. Thus, it is expected that the adsorbed dithiolates interfere with the Au−COO bond and

induce an orientation change of dangling citrate anions through vdW interactions with adjacent alkyl chains. The IR data are consistent with this hypothesis (Figure 6A). For 1,3-alkanedithiol, the IR feature in the ν(C═O) region is mostly similar to that for alkanethiolates because the 1,3-alkanedithiolate size is much smaller than the vacant area and the dithiolates can diffuse on the surface with negligible disruption of adsorbed citrate. For 1,6-alkanedithiol, however, the ν(C═O) at 1704 cm^{-1} associated with dangling citrate is substantially decreased and $\nu(COO^-)$ bands of Au−COO are broadened. Figure 6B presents a structural model suggesting that the 1,6-alkanedithiolate molecule is tightly confined in a vacant area on the Au surface but also, through diffusion, may severely disrupt the original orientation of hydrogen-bonded dangling anions leading to a standing-up configuration (inset, Figure 6B). This perpendicular orientation of the COOH dimer plane makes the ν(C═O) dipole IR-inactive, as discussed previously (Figure 1A). For 1,9-alkanedithiolate, adsorption of one sulfur atom may be dominant,[69] and the intensity of the ν(C═O) at 1704 cm^{-1} is recovered to some extent, with the feature of $\nu(COO^-)$ bands around 1540−1640 cm^{-1} being similar to that of 1,3-alkanedithiolate. The slight shift of the peak at 1704 to ~1710 cm^{-1} may reflect the intramolecular hydrogen bonding between the terminal COOH and the central hydroxyl group for dangling citrate (Table S1). The increase in transmittance magnitude of the 1734 cm^{-1} band may arise by orientation change of the acyclic COOH dimer. The unique IR data from 1,6-alkanedithiolate adsorption are evidence of the presence of a certain area of surface vacancy in the 2-D citrate network. Consequently, the size-specific vacancy is indirect evidence of vdW contact between citrate $-CH_2-$ fragments.

The inset in Figure 5B illustrates an overall structure of thiolate layers on an icosahedral Cit-AuNP. A group of four thiolate molecules form a mixed layer, with the remaining citrate anions on facets, whereas thiolates can form dense layers at edges and vertexes[65] where acetoacetate and non-hydrogen-bonded citrate anions are completely displaced by thiols. Due to the remaining citrate layer with a thickness of 8−10 Å, interparticle spacing less than 1 nm cannot be achieved, and this is supported by the experimental observation that Cit-AuNP aggregation in ethanol solution does not occur even when HS−C_3−SH and HS−C_4−SH dithiol linkers are applied.[11] Moreover, nonmonotonic behavior of thiol-functionalized Cit-AuNPs is highly possible, which depends on both molecular length and terminal functionality. When the hydrogen bond of one end of the dangling citrate species is disrupted due to a partial deprotonation of carboxylic acid groups in a neutral pH condition or as a consequence of molecular interactions, the terminal carboxylate group of citrate anions can reach a distance of 14 Å above the metal surface (inset in Figure 6B). This thickness is comparable with 1-octanethiolate fully extended from the surface. The stretched dangling citrates at the outermost ligand layer promote interparticle attraction through interlayer hydrogen bonding.[11] We predict a similar behavior of the thiolate adsorption on Cit-AgNPs. Overall, the inhomogeneous ligand layers on AuNPs can provide insight into molecular effects of local-curvature-dependent packing density of thiolates as well as the resulting flexibility, morphology, and surface charge of the ligand layer. This detailed study of molecular overlayers on large AuNPs may provide clearer understanding of NPs for interparticle assembly,[70] interactions with lipid bilayers,[71] and intracellular uptake.[72]

Origin of the Strong Adsorption of Citrates on AuNP Surfaces. The preconception for the easy displacement of adsorbed citrate by thiol is based on the difference in the chemisorption energy on a Au surface. The bond strength of thiolates (Au−S) is about 40 kcal/mol, whereas the Au−O_{COOH} bond strength is about 2 kcal/mol, for which the latter was estimated by conductance values of molecular junctions.[9] Unlike the monodentate form of citrate adsorption, however, intermolecular interactions between surface citrates play an important role in the strong adsorption of citrate on AuNPs. Particularly, the strength of hydrogen bonds of carboxylic acid groups between adjacent citrates is remarkable (~7 kcal/mol per bond of carboxylic acid dimers at room temperature)[73] compared to the single Au−O_{COOH} interaction. Although the low surface coverage of the hydrogen-bonded citrate species on AuNPs[11] allows the potentially vacant surface area to be sufficient for adsorption of incoming ligands, the enthalpy gain from intermolecular interactions of surface citrates leads to a significant barrier to spontaneous desorption in a ligand exchange process. Thus, a facile citrate-to-thiol exchange does not necessarily occur on the AuNP surface. The pervasive assumption about citrate displacement based on the weak gold−carboxylate interaction fails to accurately describe the ligand exchange process.

The coadsorbed thiolates and citrates lead to the formation of a closely packed mixed layer on AuNPs. The structural model of citrate adsorption on gold surfaces suggested that the spacing of $-CH_2-$ moieties between adjacent adsorbed citrates is within contact distance for vdW attraction (5.0−5.8 Å). Steric hindrance of the consequent layer likely prevents incoming thiols from binding to the metal surface. This makes ligand exchange kinetically unfavorable. Murray and co-workers found that most of the ligand exchange reactions between adsorbed and incoming thiols on gold clusters occur fast at vertex and edge sites, whereas the exchange reactions on terrace sites are very slow.[74] When the high ratio of terrace sites on the large AuNPs is taken into consideration, the

citrate-to-thiolate exchange may not practically occur on facets once the vacant areas are occupied by thiols. Even polynuclear iron(III)−citrate complexes exhibit slower dissociation of citrate by incoming ligands than do di- or trinuclear species due to the steric effect.[75] For the phosphine-to-thiol exchange, Hutchison and co-workers demonstrated complete displacement of the adsorbed triphenylphosphine (PPh_3) by incoming thiols using NMR spectroscopy.[76] This facile ligand exchange occurs due to negligible terrace sites and negated steric hindrance in the small nanocrystals (1.5 nm) as well as a lack of strong intermolecular interactions between phosphines. For the citrate-to-thiol exchange, the complete exchange reaction occurs for acetoacetate and non-hydrogen-bonded citrate anions mostly at vertex and edge sites. In addition to the steric hindrance, the chelate effect of the entire network of citrate layers can play a critical role in adsorption strength of the polydentate citrate on a surface.

Surface Composition and Anion Organization at the Metal Surface. The study of the citrate-to-thiol ligand exchange enables us to suggest a detailed surface composition and structure for as-prepared Cit-AuNPs. In a previous study, we estimated that the composition ratio of acetoacetic acid to surface citrate was ~2.3 by analyzing the intensity ratio of XPS C 1s for carbonyl and carboxyl carbons. However, the ratio can deviate significantly, depending on the degree of protonation of carboxylic acid groups. For instance, the composition ratio changes from 2.3 to 1.2 upon considering a deprotonated form of acetoacete in the XPS analysis (see page S18 in ref 11). Epple and co-workers precisely determined a surface density of 3.1 citrates/nm^2, by elemental analyses of carbon, hydrogen, and gold for Cit-AuNPs with a diameter of 17−20 nm.[35] This yields ~5.5 citrate anions per unit cell of 179 $Å^2$, approximately equivalent to a total of three citrate and three acetoacetate anions. Their experimental result is in good agreement with our XPS analyses and citrate assembly model.

We also indentify chemical species of chloride ions as Cl^- adsorbed on metallic Au(0) surfaces. Gold chloride Au(I)−Cl^- may be present on the AuNP surface, but we considered partial charge transfer from chloride ions to metallic gold atoms.[77] The XPS Au 4f spectrum of as-prepared Cit-AuNPs fits with inclusion of negative gold ions, that is, the Au(−1) state,[78] and this fraction is not negligible since the Au 4f ratio of Au(−1)/Au(+1) is 0.9 (Figure S18 in the Supporting Information). This is consistent with the unusually high BE of Cl $2p_{3/2}$ at 200.3 eV (Figure S7 in the Supporting Information). While charge transfer from metallic Au(0) surfaces to Cl adatoms occurs due to the high electronegativity of Cl,[45] XPS Au 4f and Cl 2p spectra in this study support charge transfer from Cl^- to metallic Au(0). Using eq 6 results in 1.4 chlorides/nm^2, only by incorporating the peak areas of Cl $2p_{3/2}$ at 200.3 eV with its doublet. Adsorption strength of Cl^- is comparable to those of oxyanions such as SO_4^{2-} and OH^-.[39] The large value of surface coverage by chloride ions may reflect the high solution concentration of chloride ions.[38]

TABLE 1. Surface Chemical Composition of Cit-AuNPs before/after Thiol Functionalization

		Cit-AuNP as-prepared	after functionalization
surface metals[a] (%)	Au(0)	86[b]	70[c]
	Au(I)	14	30 ± 2.9
overlayers[d] (molecules/nm^2)	citrate[e]	1.7	1.7
	acetoacetate[e]	1.7	0
	chloride[f]	1.4	0
	thiol		2.2−3.1[g]

[a] Au(III) content was not included: <2%. [b] Au(−1) fraction is included. [c] Oxidized once exposed to ethanol solutions. [d] Species directly adsorbed on the metal surface are presented. [e] Based on the carbon content in ref 35. This value may be overestimated due to possible physisorption of organic residues in the citrate/acetoacetate layer. [f] The observed XPS ratio of Cl^- to Au(−1) is 0.8. Only Au(0)−Cl^- species are included. [g] Dependent on the degree of which organization of dangling citrates is disrupted by thiol functional groups.

Another striking outcome applying eq 6 to alkanethiolate-functionalized AuNPs is the fraction of oxidized gold atoms Au(I) of 0.30 ± 0.03, that is, Au(I)/(Au(I) + 0.33 × Au(0)), taking into account only the outermost metallic layers. In other words, one of every three surface gold atoms is oxidized. Once Cit-AuNPs are exposed to solution, the Au(I) fractions become constant irrespective of the amount of thiolates adsorbed on the AuNPs (Figure S19 in the Supporting Information), suggesting that thiol adsorption does not oxidize surface gold atoms. For as-prepared Cit-AuNPs, the surface fraction of Au(I) oxidation state is 0.14, and hence, the oxidation states of the AuNP surface and a pristine gold surface are quite different. Positively charged metal surfaces of AuNPs may enhance adsorption stability of citrate, and consequently, the extent of surface gold oxidation may be well-balanced with citrate organization.

It is surprising that the determination of the surface composition of Cit-AuNPs is scarce in the literature. We used the report by Epple and co-workers in order to discern the coverage fraction of citrate from acetoacetate for Cit-AuNPs. Table 1 summarizes the surface compositions of Cit-AuNPs as prepared and upon thiol functionalization.

Figure 7 presents the most probable structure of overlayers on the Cit-AuNP surface. The surface coverage by citrate/acetoacetate anions based on the report by Epple and co-workers is about 1 ML, contrary to the high coverage by chloride ions in this study (Figure 7A). The two experimental results can be reconciled by incorporating an additional layer of citrate/acetoacetate anions physisorbed on top of the adsorbate layer in direct contact with the metal surface. Epple and

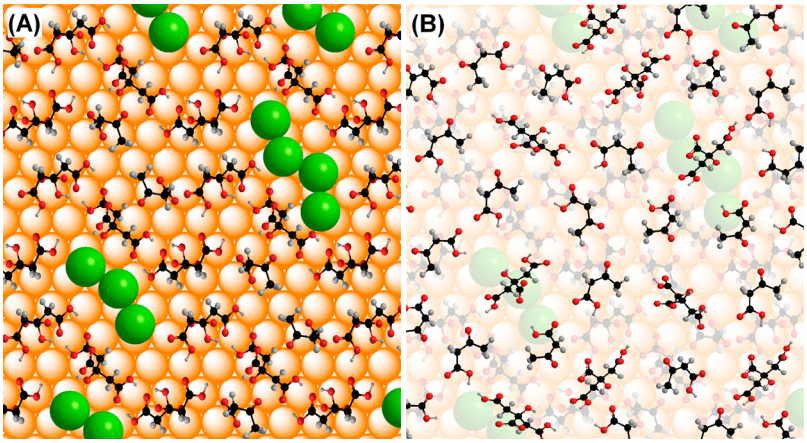

Figure 7. Proposed structure of overlayers on the Au(111) surface of Cit-AuNPs. (A) Adsorbate overlayers in direct contact with the metal surface (orange spheres), which consist of citrate, acetoacetate, and chloride anions (green spheres). Gold atoms and chloride ions are illustrated as a space-filling model. Surface Au(I) locations are unknown. The Au(100) surface may exhibit a similar structure of overlayers. (B) Physisorbed organic layer on top of the adsorbate layer, which is likely remaining on the AuNPs without extensive purification procedures. Na^+ ions, additional Cl^- ions, acetate anions, and water molecules are also present but omitted for clarity.

co-workers removed most of the water solvent from the as-prepared Cit-AuNP solution by using an evaporator. After this step, most of the acetone byproducts were likely eliminated, but other byproducts, including acetoacetate, acetate, and chloride ions, remained in the condensed AuNP solution. In a subsequent purification, they dispersed the resulting AuNP solution in water and then centrifuged for elemental analysis. In the final centrifuged AuNPs, relatively large organic anions, such as citrate and acetoacetate, might be physisorbed and trapped between the AuNPs (Figure 7B). This may result in an overestimated value of surface coverage by organic anions. In a previous study, we applied one cycle of centrifugation to obtain the sample of as-prepared Cit-AuNPs, likely having additional organic layers.[11]

Based on the model of citrate assembly, two or three molecules of acetatoacetate can be adsorbed at surface regions free of adsorbed citrate (Figure 7A). The size of a chloride ion used in this model is ~1.8 Å,[44] and on this basis, we estimate that up to four Cl^- ions may be adsorbed in the unit cell on Au(111). Considering partial charge transfer to gold surfaces, the actual size of Cl^- adsorbed on the surface may be smaller than 1.8 Å, and thus, more than four Cl^- ions can be present at the vacant area per unit cell. The overlayer structure on Au(100) may exhibit a similar arrangement, and the disordered citrate layer may exist to some extent for both facets. Due to the positively charged gold surface, anions rather than the water solvent or Na^+ ions are expected to be adsorbed on the surface of the AuNPs.[79] If the charge of the metal surface was neutral, water adsorption would be dominant.[79]

CONCLUSION

We demonstrated that citrate anions preadsorbed on AuNPs are not readily displaced by incoming aryl and alkyl thiols. Due to the stable network of hydrogen-bonded dihydrogen citrate species, coadsorption of thiols on facet areas occurs rather than a facile ligand exchange. Intermolecular interactions and consequent steric and chelating effects of the entire citrate layer are taken into account for the strong adsorption of citrate anions under thiol functionalization, although the $Au-O_{COO-}$ bond is much weaker than the Au−S bond. The primary factor of the difference in single bond energies is not sufficient to predict ligand exchange processes for metal nanoparticles.

Residual citrate anions were probed by unique IR frequencies of carboxylic acid dimerization on the AuNP surface, which is distinguished from acetoacetate, as well as carboxylate coordinated to Au atoms ($Au-COO^-$). IR and XPS data indicate that ligand exchange mainly occurs between thiols and acetoacetate anions. The coverage ratio of coadsorbed alkanethiolates ($CH_3-(CH_2)_n-S-$) to remaining citrates is 1.7 for ~40 nm Cit-AuNPs, determined by plotting XPS intensity ratios of $C_{1s}(CH_2)/C_{1s}$(citrate) with respect to the CH_2 unit (n). The atomic composition ratio of sulfur atoms (S 2p) to outermost gold atoms (Au 4f) suggests that packing densities of various alkyl/aryl thiolates range from 0.5−0.65 ML (monolayer) compared to a common SAM of 1 ML coverage on planar gold surfaces, depending on the extent of interaction between thiol functional groups and dangling citrate anions. We found that the packing density is independent of the chain length of alkanethiolates at least up to dodecanethiol. The structure-based model of citrate/thiolate coadsorption on Au(111) and Au(100) is in excellent agreement with the experimental results of citrate/thiolate and thiolate/gold(surface) composition ratios. The predicted upper limit of surface density of thiols on Cit-AuNPs is 3.1 thiolates/nm^2 (0.69 ML). The structural modeling and quantitative XPS analyses

suggest that thiol functionalization on Cit-AuNPs produces a less dense layer of thiolates on AuNPs. IR data suggest that hydrocarbon chains of alkanedithiolates exert repulsive vdW forces, making dangling citrates orient outward from the surface at the expense of citrate hydrogen bonding. Our study highlights the detailed structural characterization of buried metal/organic interfaces for large AuNPs that have been functionalized with various thiols for fundamental studies and biomedical applications. Consistent with this study and the literature, a surface chemical composition for citrate, acetoacetate, and chloride adsorbed on the metal surface of Cit-AuNPs as well as surface fraction of Au(I) oxidation state was proposed.

Intermolecular hydrogen bonds between adsorbed surfactants should be considered carefully in conjunction with adsorption strength of anchoring moieties.[80] SAMs consisting of weakly coordinated 1,2-dicarboxylic[11] and possibly phosphonic acids[81] or phosphate-based molecules on gold surfaces can be effective when strong hydrogen bonding produces a formation of network layers. This can be an alternative approach for thiol-based molecular layers that are subject to oxidation under ambient conditions and desorb from surfaces.[1,2] This study can open avenues for exploring methodologies toward formation of stable SAMs on noble metal surfaces using low-cost, non-oxidizing carboxylate or phosphate/phosphonate compounds.

METHODS

Materials. All chemicals were used as received without further purification unless otherwise stated. Tetrachloroaurate ($HAuCl_4 \cdot 3H_2O$), trisodium citrate ($Na_3C_6H_5O_7 \cdot 2H_2O$), 1-butanethiol (99%), 1-hexanethiol (95%), 1-heptanethiol (98%), 1-octanethiol (98.5%), 1-decanethiol (96%), 1-undecanethiol (98%), 1-dodecanethiol (98%), 1,3-propanedithiol (99%), 1,6-hexanedithiol (96%), and 4-mercaptopyridine (95%) were purchased from Sigma-Aldrich. 4-Nitrothiophenol (99%), 11-mercaptoundecyl trifluoroacetate (99%), 1,9-nonanedithiol (99%), and methoxy-capped tetra(ethylene glycol) undecanethiol (99%, $HS(CH_2)_{11}(OCH_2CH_2)_4OCH_3$) were obtained from Asemblon (Redmond, WA). Ethanol (EtOH, 200 proof, Pharmco-Aaper or Decon Laboratories) and sodium hydroxide (NaOH, Mallinckrodt Chemicals) were obtained from aforementioned companies. Water was used after purification (Barnstead Nanopure Diamond UV-UF, 17.8 MΩ/cm). All glassware was washed with aqua-regia (3:1, HCl/HNO_3) to remove gold particles and organic contaminants. Glassware contaminated heavily with organic materials and silicon wafers (Silicon Inc.) were cleaned with piranha solution (5:1, H_2SO_4/30% H_2O_2). *Caution! The piranha and aqua-regia solutions are highly corrosive, and mixing the solution is very exothermic. It should be handled with extreme care and appropriate safety precautions*. The aqua-regia or piranha-treated glassware was rinsed copiously with water and dried in an oven at 120 °C at least for 2 h.

Cit-AuNP Synthesis. AuNPs were synthesized using the Frens method.[11] Briefly, $HAuCl_4 \cdot 3H_2O$ (0.0232 g) was dissolved in water (200 mL), and Na_3citrate $\cdot 2H_2O$ (0.0227 g) was dissolved in water (1 mL) and added to the boiling gold salt solution all at once with stirring. Heating continued for an additional hour, and the resulting AuNP solution was cooled to room temperature with continuous stirring. The final AuNPs have an average diameter of 39 nm with ~25% deviation and exhibit an absorption maximum (λ_{max}) at 535 nm.

Addition of Thiol Solutions to Cit-AuNPs. Typically, 10 mL of the 39 nm AuNP solution in a tube was centrifuged once at 4000 rpm for ~30 min, and the resulting supernatant solution was discarded by using a pipet without disturbing aggregated AuNPs at the bottom of the tube. The rest of the centrifuged AuNPs (final volume <50 μL) were added to freshly prepared 10 mL of 1 mM ethanolic thiol solution and then sonicated for dispersion. The added thiol amount is estimated to be about 270 molar equiv for monolayer formation on AuNPs. The reaction mixture was left at room temperature for more than 2 h without stirring. The functionalized AuNPs were centrifuged and dispersed in ethanol three times to remove displaced citrates and excess thiols present in solution. Obviously, thiols (R−SH) initially physisorbed on the surface of AuNPs are transformed into thiolates ($R-S^-$) for Au−S bond formation, and this was confirmed in this study because, typically, no ν(S−H) vibration around 2560 cm^{-1} was observed (data not shown) and XPS S 2p spectra for functionalized AuNPs exhibited only thiolate species[2] (Figures S10 and S11 in the Supporting Information). The resulting ~100 μL solution of AuNPs was used to prepare samples for IR and XPS analyses.

Adsorption Isotherm of Arylthiolates on AuNPs. To study the early stages of adsorption of 4-mercaptopyridine (Py−SH) on Cit-AuNPs, ligand exchange reactions were performed, similar to the protocol described above but using different thiol concentrations. With addition of a small amount of thiol ($1/6 \le x \le 1.00$, for a monolayer coverage, $x = 1.00$), a fractional surface area smaller than the entire surface of AuNPs can be functionalized. A sphere with a diameter of 35 nm (calculated surface area = 3.8×10^{-11} cm^2) and the packing density of 4.3×10^{14} benzenethiols/cm^2 were used to calculate the fractional amounts of Py−SH to be added. This estimation does not account for deviations in the particle size. The number of AuNPs in solution was estimated using the extinction coefficient for 35 nm in the literature (6.1×10^9 $M^{-1}cm^{-1}$).[82] Six tubes each containing 10 mL of as-prepared Cit-AuNP solution were centrifuged once. The resulting AuNPs that aggregated at the bottom of all six tubes were collected and redispersed in a vial containing ~4 mL of ethanol. The final volume of the AuNP solution redistributed from six tubes was adjusted to 6.0 mL. AuNP loss of 25% during the initial centrifugation was corrected by measuring the absorbance. Into ~1.0 mL of redispersed AuNP solution in ethanol were added 268 μL ($x = 1/6$), 2×268 μL ($x = 2/6$), 3×268 μL ($x = 3/6$), 4×268 μL ($x = 4/6$), 5×268 μL ($x = 5/6$), and 6×268 μL ($x = 6/6$) of 1.4×10^{-5} M of Py−SH ethanolic solution all at once. The final volume of each solution was adjusted to 2.61 mL by adding the decremented volume of ethanol, and the resulting solution was left at room temperature for 72 h. The functionalized AuNP solution was centrifuged once without further redispersion and centrifugation steps to minimize possible desorption of the arylthiol. The final volume of centrifuged AuNP solution is less than 100 μL, and thus, the amount of leftover thiols in the collected solution is negligible.

UV−Vis Absorption Spectroscopy. Absorbance of AuNP solution was collected for a spectral range of 400−800 nm using a PerkinElmer Lambda 19 UV/vis/NIR spectrophotometer.

Attenuated Total Reflectance Infrared Spectroscopy. A PerkinElmer Spectrum 100 Fourier transform infrared spectrometer equipped with a MIRacle ATR (ZnSe crystal, PIKE Technologies) accessory was used. Centrifuged AuNP solution was transferred onto the crystal and dried with nitrogen gas. Spectra were collected at 4000−550 cm^{-1} after ethanol in the samples had evaporated. ATR spectra were not baseline-corrected. Deconvolution was performed by peak fitting analysis using Lorentzian or Voigt functions in OriginPro 8.5.

X-ray Photoelectron Spectroscopy. X-ray photoelectron spectra were collected using a monochromatic Al Kα source (1486.6 eV)

with a power of 144 W on a Kratos Axis Ultra DLD instrument (Chestnut Ridge, NY) without sputtering. The base pressure was 2×10^{-9} Torr. The incidence angle of the incoming X-ray was 54.7°, and the electron takeoff angle was 90°. Typically, the X-ray beam generates a 300 × 700 μm^2 spot size. A drop-cast film of the functionalized AuNPs was prepared on silicon wafers, and complete coverage of the AuNP film was identified by the absence of Si peaks. Survey spectra were recorded with the pass energy of 160 eV (1 eV steps, 200 ms dwell), and high-resolution spectra at energy ranges of interest were recorded with a pass energy of 40 eV (0.1 eV, 400 ms dwell). The binding energies shifted by substrate charging were corrected by referencing the C 1s peak of adventitious carbon to 284.8 eV. Data analysis was performed with CasaXPS software. The background was subtracted by the linear or Shirely's method, which was used as a baseline for determining peak areas. Each deconvolution into component peaks was performed with an identical full width at half-maximum. XPS peak areas for S 2p and Au 4f were obtained including spin−orbit doublets. Au(+1) oxidized species at a lower BE was included in peak areas of Au 4f. Typically, S $2p_{3/2}$ = 162 eV and Au $4f_{7/2}$ = 84.0 eV along with Au(+1) $4f_{7/2}$ = 84.7 eV. Relative atomic compositions were obtained from dividing peak areas by XPS sensitivity factors. Those relative intensities were used in XPS plots.

Modeling. A structural model of molecular adsorption on Au(111) was constructed with molecules accurately scaled to the Au−Au interatomic spacing of 2.88 Å, as described in a previous study.[11] Briefly, Au_2-citrate clusters were generated by a ChemBio3D program and used for scaling on Au(111). Molecules' 3-D structures are snapshots captured in ChemBio3D.

Conflict of Interest: The authors declare no competing financial interest.

Acknowledgment. We thank Brian van Devener from the Surface Analysis Laboratory at the University of Utah for assistance in XPS experiments. This work was supported by the National Science Foundation through an NSF Career Award (Grant No. CHE-0844764).

Supporting Information Available: Additional UV−vis, XPS, and IR spectra as well as figure of dangling citrate orientation, summary of ν(C═O) frequencies of citrate species, apparent S_{2p}/Au_{4f} and C_{1s}(carboxyl)/Au_{4f} values for Cit-AuNPs functionalized with various thiols, supplementary discussion relating to Figure 4B, selected S_{2p}/Au_{4f} values for citrate-free AuNPs functionalized with thiols in the literature, a diagram relating to eq 6, surface coverage of various thiols, and apparent Au(I)/Au(0) ratios. This material is available free of charge *via* the Internet at http://pubs.acs.org.

REFERENCES AND NOTES

1. Love, J. C.; Estroff, L. A.; Kriebel, J. K.; Nuzzo, R. G.; Whitesides, G. M. Self-Assembled Monolayers of Thiolates on Metals as a Form of Nanotechnology. *Chem. Rev.* **2005**, *105*, 1103–1169.
2. Vericat, C.; Vela, M. E.; Benitez, G.; Carro, P.; Salvarezza, R. C. Self-Assembled Monolayers of Thiols and Dithiols on Gold: New Challenges for a Well-Known System. *Chem. Soc. Rev.* **2010**, *39*, 1805–1834.
3. Nuzzo, R. G.; Allara, D. L. Adsorption of Bifunctional Organic Disulfides on Gold Surfaces. *J. Am. Chem. Soc.* **1983**, *105*, 4481–4483.
4. Porter, M. D.; Bright, T. B.; Allara, D. L.; Chidsey, C. E. D. Spontaneously Organized Molecular Assemblies. 4. Structural Characterization of *n*-Alkyl Thiol Monolayers on Gold by Optical Ellipsometry, Infrared Spectroscopy, and Electrochemistry. *J. Am. Chem. Soc.* **1987**, *109*, 3559–3568.
5. Weisbecker, C. S.; Merritt, M. V.; Whitesides, G. M. Molecular Self-Assembly of Aliphatic Thiols on Gold Colloids. *Langmuir* **1996**, *12*, 3763–3772.
6. Giersig, M.; Mulvaney, P. Preparation of Ordered Colloid Monolayers by Electrophoretic Deposition. *Langmuir* **1993**, *9*, 3408–3413.
7. Dahl, J. A.; Maddux, B. L. S.; Hutchison, J. E. Toward Greener Nanosynthesis. *Chem. Rev.* **2007**, *107*, 2228–2269.
8. Nuzzo, R. G.; Zegarski, B. R.; Dubois, L. H. Fundamental Studies of the Chemisorption of Organosulfur Compounds on Gold(111). Implications for Molecular Self-Assembly on Gold Surfaces. *J. Am. Chem. Soc.* **1987**, *109*, 733–740.
9. Chen, F.; Li, X.; Hihath, J.; Huang, Z.; Tao, N. Effect of Anchoring Groups on Single-Molecule Conductance: Comparative Study of Thiol-, Amine-, and Carboxylic-Acid-Terminated Molecules. *J. Am. Chem. Soc.* **2006**, *128*, 15874–15881.
10. Huheey, J. E.; Keiter, E. A.; Keiter, R. L. *Inorganic Chemistry: Principles of Structure and Reactivity*, 4th ed.; Harper Collins College Publishers: New York, 1993.
11. Park, J.-W.; Shumaker-Parry, J. S. Structural Study of Citrate Layers on Gold Nanoparticles: Role of Intermolecular Interactions in Stabilizing Nanoparticles. *J. Am. Chem. Soc.* **2014**, *136*, 1907–1921.
12. Larson, I.; Chan, D. Y. C.; Drummond, C. J.; Grieser, F. Use of Atomic Force Microscopy Force Measurements To Monitor Citrate Displacement by Amines on Gold in Aqueous Solution. *Langmuir* **1997**, *13*, 2429–2431.
13. Wall, J. F.; Grieser, F.; Zukoski, C. F. Monitoring Chemical Reactions at the Gold/Solution Interface Using Atomic Force Microscopy. *J. Chem. Soc., Faraday Trans.* **1997**, *93*, 4017–4020.
14. Kim, B. Y. S.; Rutka, J. T.; Chan, W. C. W. Nanomedicine. *N. Engl. J. Med.* **2010**, *363*, 2434–2443.
15. Nel, A. E.; Mädler, L.; Velegol, D.; Xia, T.; Hoek, E. M. V.; Somasundaran, P.; Klaessig, F.; Castranova, V.; Thompson, M. Understanding Biophysicochemical Interactions at the Nano−Bio Interface. *Nat. Mater.* **2009**, *8*, 543–557.
16. Taylor, U.; Rehbock, C.; Streich, C.; Rath, D.; Barcikowski, S. Rational Design of Gold Nanoparticle Toxicology Assays: A Question of Exposure Scenario, Dose and Experimental Setup. *Nanomedicine* **2014**, *9*, 1971–1989.
17. Petersen, S.; Barcikowski, S. Conjugation Efficiency of Laser-Based Bioconjugation of Gold Nanoparticles with Nucleic Acids. *J. Phys. Chem. C* **2009**, *113*, 19830–19835.
18. Weitz, D. A.; Oliveria, M. Fractal Structures Formed by Kinetic Aggregation of Aqueous Gold Colloids. *Phys. Rev. Lett.* **1984**, *52*, 1433–1436.
19. Newman, J. D. S.; MacCrehan, W. A. The Effect of Aniline Concentration in the Ligand Exchange Reaction with Citrate-Stabilized Gold Nanoparticles. *Langmuir* **2009**, *25*, 8993–8998.
20. Zakaria, H. M.; Shah, A.; Konieczny, M.; Hoffmann, J. A.; Nijdam, A. J.; Reeves, M. E. Small Molecule- and Amino Acid-Induced Aggregation of Gold Nanoparticles. *Langmuir* **2013**, *29*, 7661–7673.
21. Dagastine, R. R.; Grieser, F. Dynamics of the Interaction Forces at the Silver/Solution Interface during Amine Adsorption. *Langmuir* **2004**, *20*, 6742–6747.
22. Zhong, Z.; Patskovskyy, S.; Bouvrette, P.; Luong, J. H. T.; Gedanken, A. The Surface Chemistry of Au Colloids and Their Interactions with Functional Amino Acids. *J. Phys. Chem. B* **2004**, *108*, 4046–4052.
23. Matsunaga, M.; Aizenberg, M.; Aizenberg, J. Controlling the Stability and Reversibility of Micropillar Assembly by Surface Chemistry. *J. Am. Chem. Soc.* **2011**, *133*, 5545–5553.
24. Arnold, R.; Azzam, W.; Terfort, A.; Wöll, C. Preparation, Modification, and Crystallinity of Aliphatic and Aromatic Carboxylic Acid Terminated Self-Assembled Monolayers. *Langmuir* **2002**, *18*, 3980–3992.
25. Doyen, M.; Bartik, K.; Bruylants, G. UV−Vis and NMR Study of the Formation of Gold Nanoparticles by Citrate Reduction: Observation of Gold-Citrate Aggregates. *J. Colloid Interface Sci.* **2013**, *399*, 1–5.
26. Wang, J.-g.; Selloni, A. First Principles Study of Fatty Acid Monolayers on Au(111). *J. Phys. Chem. C* **2009**, *113*, 8895–8900.
27. Devlin, J. P.; Consani, K. Metal Surface Spectroscopy. Charge Transfer and Totally Symmetric Mode Activity. *J. Phys. Chem.* **1981**, *85*, 2597–2598.
28. Skibbe, O.; Binder, M.; Otto, A.; Pucci, A. Electronic Contributions to Infrared Spectra of Adsorbate Molecules on

Metal Surfaces: Ethene on Cu(1 1 1). *J. Chem. Phys.* **2008**, *128*, 194703.
29. Leung, T. Y. B.; Gerstenberg, M. C.; Lavrich, D. J.; Scoles, G.; Schreiber, F.; Poirier, G. E. 1,6-Hexanedithiol Monolayers on Au(111): A Multitechnique Structural Study. *Langmuir* **2000**, *16*, 549–561.
30. Sastry, M.; Ganguly, P. Determination of C 1s Core Level Chemical Shifts in Some Langmuir–Blodgett Films Using a Modified Sanderson Formalism. *J. Phys. Chem. A* **1998**, *102*, 697–702.
31. Lin, N.; Payer, D.; Dmitriev, A.; Strunskus, T.; Wöll, C.; Barth, J. V.; Kern, K. Two-Dimensional Adatom Gas Bestowing Dynamic Heterogeneity on Surfaces. *Angew. Chem., Int. Ed.* **2005**, *44*, 1488–1491.
32. Zhang, Z.; Wu, Y. Investigation of the $NaBH_4$-Induced Aggregation of Au Nanoparticles. *Langmuir* **2010**, *26*, 9214–9223.
33. Duan, J.; Linman, M. J.; Chen, C.-Y.; Cheng, Q. J. CHCA-Modified Au Nanoparticles for Laser Desorption Ionization Mass Spectrometric Analysis of Peptides. *J. Am. Soc. Mass Spectrom.* **2009**, *20*, 1530–1539.
34. Zhang, S.; Leem, G.; Srisombat, L.; Lee, T. R. Rationally Designed Ligands that Inhibit the Aggregation of Large Gold Nanoparticles in Solution. *J. Am. Chem. Soc.* **2008**, *130*, 113–120.
35. Rostek, A.; Mahl, D.; Epple, M. Chemical Composition of Surface-Functionalized Gold Nanoparticles. *J. Nanopart. Res.* **2011**, *13*, 4809–4814.
36. Xue, C.; Métraux, G. S.; Millstone, J. E.; Mirkin, C. A. Mechanistic Study of Photomediated Triangular Silver Nanoprism Growth. *J. Am. Chem. Soc.* **2008**, *130*, 8337–8344.
37. Borer, P.; Hug, S. J.; Sulzberger, B.; Kraemer, S. M.; Kretzschmar, R. Photolysis of Citrate on the Surface of Lepidocrocite: An *in Situ* Attenuated Total Reflection Infrared Spectroscopy Study. *J. Phys. Chem. C* **2007**, *111*, 10560–10569.
38. Balasubramanian, S. K.; Yang, L.; Yung, L.-Y. L.; Ong, C.-N.; Ong, W.-Y.; Yu, L. E. Characterization, Purification, and Stability of Gold Nanoparticles. *Biomaterials* **2010**, *31*, 9023–9030.
39. Chen, A.; Lipkowski, J. Electrochemical and Spectroscopic Studies of Hydroxide Adsorption at the Au(111) Electrode. *J. Phys. Chem. B* **1999**, *103*, 682–691.
40. Sylvestre, J.-P.; Poulin, S.; Kabashin, A. V.; Sacher, E.; Meunier, M.; Luong, J. H. T. Surface Chemistry of Gold Nanoparticles Produced by Laser Ablation in Aqueous Media. *J. Phys. Chem. B* **2004**, *108*, 16864–16869.
41. Wang, X.; Andrews, L. Infrared Spectrum and Structure of the Gold Dihydroxide Molecule. *Chem. Commun.* **2005**, 4001–4003.
42. Green, I. X.; Tang, W.; Neurock, M.; Yates, J. T., Jr. Mechanistic Insights into the Partial Oxidation of Acetic Acid by O_2 at the Dual Perimeter Sites of a Au/TiO_2 Catalyst. *Faraday Discuss.* **2013**, *162*, 247–265.
43. Shchukarev, A.; Boily, J.-F.; Felmy, A. R. XPS of Fast-Frozen Hematite Colloids in NaCl Aqueous Solutions: I. Evidence for the Formation of Multiple Layers of Hydrated Sodium and Chloride Ions Induced by the {001} Basal Plane. *J. Phys. Chem. C* **2007**, *111*, 18307–18316.
44. Kastanas, G. N.; Koel, B. E. Interaction of Cl_2 with the Au(111) Surface in the Temperature Range of 120 to 1000 K. *Appl. Surf. Sci.* **1993**, *64*, 235–246.
45. Gao, W.; Baker, T. A.; Zhou, L.; Pinnaduwage, D. S.; Kaxiras, E.; Friend, C. M. Chlorine Adsorption on Au(111): Chlorine Overlayer or Surface Chloride? *J. Am. Chem. Soc.* **2008**, *130*, 3560–3565.
46. Werner, W. S. M.; Chudzicki, M.; Smekal, W.; Powell, C. J. Interpretation of Nanoparticle X-ray Photoelectron Intensities. *Appl. Phys. Lett.* **2014**, *104*, 243106.
47. Wan, L.-J.; Terashima, M.; Noda, H.; Osawa, M. Molecular Orientation and Ordered Structure of Benzenethiol Adsorbed on Gold(111). *J. Phys. Chem. B* **2000**, *104*, 3563–3569.
48. Briggs, D.; Beamson, G. Primary and Secondary Oxygen-Induced C1s Binding Energy Shifts in X-ray Photoelectron Spectroscopy of Polymers. *Anal. Chem.* **1992**, *64*, 1729–1736.
49. Dannenberger, O.; Buck, M.; Grunze, M. Self-Assembly of *n*-Alkanethiols: A Kinetic Study by Second Harmonic Generation. *J. Phys. Chem. B* **1999**, *103*, 2202–2213.
50. Tsai, D-H.; Zangmeister, R. A.; Pease, L. F., III; Tarlov, M. J.; Zachariah, M. R. Gas-Phase Ion-Mobility Characterization of SAM-Functionalized Au Nanoparticles. *Langmuir* **2008**, *24*, 8483–8490.
51. Harder, P.; Grunze, M.; Dahint, R.; Whitesides, G. M.; Laibinis, P. E. Molecular Conformation in Oligo(ethylene glycol)-Terminated Self-Assembled Monolayers on Gold and Silver Surfaces Determines Their Ability To Resist Protein Adsorption. *J. Phys. Chem. B* **1998**, *102*, 426–436.
52. Powell, C. J.; Jablonski, A. Progress in Quantitative Surface Analysis by X-ray Photoelectron Spectroscopy: Current Status and Perspectives. *J. Electron Spectrosc. Relat. Phenom.* **2010**, *178–179*, 331–346and references therein.
53. Techane, S. D.; Gamble, L. J.; Castner, D. G. Multitechnique Characterization of Self-Assembled Carboxylic Acid-Terminated Alkanethiol Monolayers on Nanoparticle and Flat Gold Surfaces. *J. Phys. Chem. C* **2011**, *115*, 9432–9441.
54. Techane, S.; Baer, D. R.; Castner, D. G. Simulation and Modeling of Self-Assembled Monolayers of Carboxylic Acid Thiols on Flat and Nanoparticle Gold Surfaces. *Anal. Chem.* **2011**, *83*, 6704–6712.
55. Bain, C. D.; Whitesides, G. M. Attenuation Lengths of Photoelectrons in Hydrocarbon Films. *J. Phys. Chem.* **1989**, *93*, 1670–1673.
56. Shard, A. G.; Wang, J.; Spencer, S. J. XPS Topofactors: Determining Overlayer Thickness on Particles and Fibers. *Surf. Interface Anal.* **2009**, *41*, 541–548.
57. Ghorai, P. K.; Glotzer, S. C. Molecular Dynamics Simulation Study of Self-Assembled Monolayers of Alkanethiol Surfactants on Spherical Gold Nanoparticles. *J. Phys. Chem. C* **2007**, *111*, 15857–15862.
58. Joseph, Y.; Besnard, I.; Rosenberger, M.; Guse, B.; Nothofer, H.-G.; Wessels, J. M.; Wild, U.; Knop-Gericke, A.; Su, D.; Schlögl, R.; et al. Self-Assembled Gold Nanoparticle/Alkanedithiol Films: Preparation, Electron Microscopy, XPS-Analysis, Charge Transport, and Vapor-Sensing Properties. *J. Phys. Chem. B* **2003**, *107*, 7406–7413.
59. Baer, D. R.; Engelhard, M. H. XPS Analysis of Nanostructured Materials and Biological Surfaces. *J. Electron Spectrosc. Relat. Phenom.* **2010**, *178–179*, 415–432.
60. Thierry, B.; Ng, J.; Krieg, T.; Griesser, H. J. A Robust Procedure for the Functionalization of Gold Nanorods and Noble Metal Nanoparticles. *Chem. Commun.* **2009**, 1724–1726.
61. Techane, S. D.; Gamble, L. J.; Castner, D. G. X-ray Photoelectron Spectroscopy Characterization of Gold Nanoparticles Functionalized with Amine-Terminated Alkanethiols. *Biointerphases* **2011**, *6*, 98–104.
62. Xia, X.; Yang, M.; Wang, Y.; Zheng, Y.; Li, Q.; Chen, J.; Xia, Y. Quantifying the Coverage Density of Poly(ethylene glycol) Chains on the Surface of Gold Nanostructures. *ACS Nano* **2012**, *6*, 512–522.
63. Ansar, S. M.; Haputhanthri, R.; Edmonds, B.; Liu, D.; Yu, L.; Sygula, A.; Zhang, D. Determination of the Binding Affinity, Packing, and Conformation of Thiolate and Thione Ligands on Gold Nanoparticles. *J. Phys. Chem. C* **2011**, *115*, 653–660.
64. Jiménez, A.; Sarsa, A.; Blázquez, M.; Pineda, T. A Molecular Dynamics Study of the Surfactant Surface Density of Alkanethiol Self-Assembled Monolayers on Gold Nanoparticles as a Function of the Radius. *J. Phys. Chem. C* **2010**, *114*, 21309–21314 and references therein.
65. Djebaili, T.; Richardi, J.; Abel, S.; Marchi, M. Atomistic Simulations of the Surface Coverage of Large Gold Nanocrystals. *J. Phys. Chem. C* **2013**, *117*, 17791–17800.
66. Nelson, E. M.; Rothberg, L. J. Kinetics and Mechanism of Single-Stranded DNA Adsorption onto Citrate-Stabilized Gold Nanoparticles in Colloidal Solution. *Langmuir* **2011**, *27*, 1770–1777.

67. Loglio, F.; Schweizer, M.; Kolb, D. M. *In Situ* Characterization of Self-Assembled Butanethiol Monolayers on Au(100) Electrodes. *Langmuir* **2003**, *19*, 830–834.
68. Scott, M. C.; Chen, C.-C.; Mecklenburg, M.; Zhu, C.; Xu, R.; Ercius, P.; Dahmen, U.; Regan, B. C.; Miao, J. Electron Tomography at 2.4-Ångström Resolution. *Nature* **2012**, *483*, 444–447.
69. Millone, M. A. D.; Hamoudi, H.; Rodríguez, L.; Rubert, A.; Benítez, G. A.; Vela, M. E.; Salvarezza, R. C.; Gayone, J. E.; Sánchez, E. A.; Grizzi, O.; et al. Self-Assembly of Alkanedithiols on Au(111) from Solution: Effect of Chain Length and Self-Assembly Conditions. *Langmuir* **2009**, *25*, 12945–12953.
70. Walker, D. A.; Leitsch, E. K.; Nap, R. J.; Szleifer, I.; Grzybowski, B. A. Geometric Curvature Controls the Chemical Patchiness and Self-Assembly of Nanoparticles. *Nat. Nanotechnol.* **2013**, *8*, 676–681.
71. Van Lehn, R. C.; Ricci, M.; Silva, P. H. J.; Andreozzi, P.; Reguera, J.; Voïtchovsky, K.; Stellacci, F.; Alexander-Katz, A. Lipid Tail Protrusions Mediate the Insertion of Nanoparticles into Model Cell Membranes. *Nat. Commun.* **2014**, *5*, 4482.
72. Lin, J.; Zhang, H.; Chen, Z.; Zheng, Y. Penetration of Lipid Membranes by Gold Nanoparticles: Insights into Cellular Uptake, Cytotoxicity, and Their Relationship. *ACS Nano* **2010**, *4*, 5421–5429.
73. Gao, Q.; Hemminger, J. C. A Vibrational Spectroscopy Study of CH_3COOH, CH_3COOD and $^{13}CD_3COOH$(D) Adsorption on Pt(111): I. Surface Dimer Formation and Hydrogen Bonding. *Surf. Sci.* **1991**, *248*, 45–56.
74. Guo, R.; Song, Y.; Wang, G.; Murray, R. W. Does Core Size Matter in the Kinetics of Ligand Exchanges of Monolayer-Protected Au Clusters? *J. Am. Chem. Soc.* **2005**, *127*, 2752–2757.
75. Gautier-Luneau, I.; Merle, C.; Phanon, D.; Lebrun, C.; Biaso, F.; Serratrice, G.; Pierre, J.-L. New Trends in the Chemistry of Iron(III) Citrate Complexes: Correlations between X-ray Structures and Solution Species Probed by Electrospray Mass Spectrometry and Kinetics of Iron Uptake from Citrate by Iron Chelators. *Chem.—Eur. J.* **2005**, *11*, 2207–2219.
76. Woehrle, G. H.; Brown, L. O.; Hutchison, J. E. Thiol-Functionalized, 1.5-nm Gold Nanoparticles through Ligand Exchange Reactions: Scope and Mechanism of Ligand Exchange. *J. Am. Chem. Soc.* **2005**, *127*, 2172–2183.
77. Kolics, A.; Thomas, A. E.; Wieckowski, A. ^{36}Cl Labelling and Electrochemical Study of Chloride Adsorption on a Gold Electrode from Perchloric Acid Media. *J. Chem. Soc., Faraday Trans.* **1996**, *92*, 3727–3736.
78. Herranz, T.; Deng, X.; Cabot, A.; Alivisatos, P.; Liu, Z.; Soler-Illia, G.; Salmeron, M. Reactivity of Au Nanoparticles Supported over SiO_2 and TiO_2 Studied by Ambient Pressure Photoelectron Spectroscopy. *Catal. Today* **2009**, *143*, 158–166.
79. Spohr, E. Molecular Simulation of the Electrochemical Double Layer. *Electrochim. Acta* **1999**, *44*, 1697–1705.
80. Crudden, C. M.; Horton, J. H.; Ebralidze, I. I.; Zenkina, O. V.; McLean, A. B.; Drevniok, B.; She, Z.; Kraatz, H.-B.; Mosey, N. J.; Seki, T.; et al. Ultra Stable Self-Assembled Monolayers of N-Heterocyclic Carbenes on Gold. *Nat. Chem.* **2014**, *6*, 409–414.
81. Cabrita, J. F.; Viana, A. S.; Montforts, F.-P.; Abrantes, L. M. Mixed Self-Assembled Monolayers of Co-Porphyrin and *n*-Alkane Phosphonates on Gold. *Surf. Sci.* **2011**, *605*, 1412–1419.
82. Liu, X.; Atwater, M.; Wang, J.; Huo, Q. Extinction Coefficient of Gold Nanoparticles with Different Sizes and Different Capping Ligands. *Colloids Surf., B* **2007**, *58*, 3–7.